

Stat3 mediated alterations in lysosomal membrane protein composition

Bethan Lloyd-Lewis^{1§}, Caroline C. Krueger^{1¥}, Timothy J. Sargeant², Michael E. D'Angelo¹, Michael J. Deery³, Renata Feret³, Julie A. Howard³, Kathryn S. Lilley³ and Christine J. Watson^{1*}

¹Department of Pathology, University of Cambridge, Cambridge, CB2 1QP, UK. ²Lysosomal Diseases Research Unit, South Australian Health and Medical Research Institute Adelaide, SA, Australia. ³Cambridge Centre for Proteomics, Department of Biochemistry, University of Cambridge, Tennis Court Road, CB2 1QR, Cambridge, UK.

Running Title: *Stat3 alters proteins in the lysosomal membrane*

§Present address: Department of Genetics and Developmental Biology, Institut Curie, Paris, France.

¥Present address: University Clinic of Rheumatology, Immunology and Allergology, Department of Immunology, Inselspital, Bern University Hospital, University of Bern, Switzerland.

*Correspondence: Professor Christine Watson, Email: cjw53@cam.ac.uk, Tel: +44 (0)1223 333725

Keywords: Proteomics, lysosome, Stat3, mammary gland, mammary epithelial cells, cell death

Abstract

Lysosome function is essential in cellular homeostasis. In addition to its recycling role, the lysosome has recently been recognised as a cellular signalling hub. We have shown in mammary epithelial cells, both *in vivo* and *in vitro*, that signal transducer and activator of transcription 3 (Stat3) modulates lysosome biogenesis and can promote the release of lysosomal proteases that culminates in cell death. To further investigate the impact of Stat3 on lysosomal function, we have conducted a proteomic screen of changes in lysosomal membrane protein components induced by Stat3 using an iron nanoparticle enrichment strategy. Our results show that Stat3 activation not only elevates the levels of known membrane proteins but results in the appearance of unexpected factors, including cell surface proteins such as annexins and flotillins. These data suggest that Stat3 may co-ordinately regulate endocytosis, intracellular trafficking and lysosome biogenesis to drive lysosomal-mediated cell death in mammary epithelial cells. The methodologies described in this study also provide significant improvements to current techniques used for the purification and analysis of the lysosomal proteome.

Introduction

Lysosomes are intracellular organelles that were first described by Christian de Duve over half a century ago, so-named from the Greek words lysis (dissolution or destruction) and soma (body)¹. The lysosome has an essential function in the digestion of old organelles, engulfed proteins and microbes that are delivered to the lysosome for degradation by autophagy, endocytosis and phagocytosis, respectively. Delivery is mediated by kissing events between lysosomes and late endosomes/multivesicular bodies, or by direct fusion of lysosomes and autophagosomes². Lysosomes can also fuse with the plasma membrane to mediate repair and exocytosis³. Sub-optimal lysosome function and reduced lysosomal clearance is associated with ageing, neurodegenerative diseases such as Alzheimer's, and lysosomal storage disorders that are caused by deficiencies in lysosomal proteins or trafficking⁴. The lysosomal lumen harbours numerous acid hydrolases that digest a wide array of cellular macromolecules and membranes with the resulting catabolites being recycled back to the cytosol⁵. Lysosomal proteases have multiple additional roles, including bone remodelling, angiogenesis, neuronal cell maintenance, cell death and cancer cell invasion⁶.

The lysosomal proteome has been investigated using a variety of mass spectrometry (MS)-based approaches, including affinity purification methods that exploit the mannose-6-

Stat3 alters proteins in the lysosomal membrane

phosphate modifications required to traffic proteins to the lysosome⁷⁻¹¹. Such approaches have enabled the identification of both known and previously uncharacterised proteins involved in lysosome biology⁸. However, sorting signals present on lysosomal membrane proteins are less amenable to purification, and difficulties in isolating pure populations of lysosomes have hindered proteomic analysis of lysosomal membrane constituents. As a result, this proteome is considered relatively incomplete¹². Traditional methods for isolating lysosomes have relied upon density centrifugation, resulting in preparations that are commonly contaminated by other organelles of similar density, including mitochondria and peroxisomes^{8,13-15}. Protein correlation profiling can partially mitigate this problem and provide information about the steady-state distribution of proteins within organelles^{16,17}. However, lysosomes can be highly heterogeneous in nature, and in biological contexts where their function is impaired or altered (e.g. in lysosomal storage disorders) changes in lysosomal buoyant density results in their redistribution across a density gradient, thus hampering their purification by differential centrifugation^{13,18,19}. To overcome these difficulties, we and others have utilised magnetic iron nanoparticles to isolate lysosomes from different cell types^{13,18,20,21}. Internalisation and delivery of nanoparticles via the endocytic pathway to lysosomes enables their isolation by magnetic chromatography. More recently, the utility of this method for LC-MS/MS analysis of cellular trafficking events has been demonstrated^{22,23}. However, the application of this methodology to specifically investigate changes in the lysosomal membrane proteome in the context of lysosomal dysfunction (including during lysosomal membrane permeabilisation (LMP)) has yet to be explored.

Components of the lysosomal membrane fulfil a number of crucial functions, including acidification of the lysosomal lumen, membrane fusion with other organelles and transport events that facilitate the transfer of macromolecules and degradation products^{12,24}. Preservation of lysosomal function requires the multicomponent vacuolar-type-ATPase to maintain the acidic luminal pH. The role of the densely glycosylated proteins LAMP1 and LAMP2, which constitute over 50% of the lysosomal membrane proteins¹², is less clear. It has been suggested that they form a glycocalyx that protects the lysosomal membrane from autolysis^{12,25}. However,

other studies indicate that they are not required simply for membrane stability¹², although glycosylation is necessary to protect LAMP1/2 from the action of lysosomal proteases²⁵. LMP, and the subsequent intracellular release of lysosomal hydrolases such as cathepsin proteases, is widely implicated in the initiation or enhancement of cell death programmes²⁶. Whilst cathepsin release may result in activation of the caspase cascade, cell death can also be initiated in a caspase-independent manner²⁷ in a process termed lysosomal-mediated programmed cell death (LM-PCD)²⁸. The mechanisms driving LMP appear to be highly cell type and context dependent, and have been observed across a wide spectrum of species including *C. elegans*²⁹. In addition to mediating cell death in pathological conditions, LM-PCD can regulate cell death under physiological conditions, such as during post-lactational regression (involution) of the mammary gland^{20,30}. This complex and highly regulated programme of cell death requires Stat3 signalling that co-ordinately upregulates the lysosomal system and abrogates expression of the endogenous cathepsin inhibitor Spi2a^{30,31}. Subsequent LMP and leakage of cathepsin proteases into the cytosol results in extensive cell death³⁰. More recently, we have shown that Stat3 activation mediates the uptake of milk fat globules that are delivered to large lysosomal vesicles for degradation²⁰. The resulting high local concentrations of free fatty acids within these structures lead to increased membrane permeability, cathepsin leakage and cell death²⁰. These events can be modelled *in vitro* using Oncostatin M (OSM) stimulation of Stat3 activity in the normal mouse mammary epithelial EpH4 cell line^{20,30}. It is unclear, however, if Stat3 signalling has a direct, modulatory effect on the lysosomal membrane proteome. Here, we utilised LC-MS/MS analysis of lysosomes isolated from OSM-stimulated or unstimulated EpH4 cells to address this question, and to provide further insights into the protein composition of lysosomal membranes during LM-PCD.

Results

Iron nanoparticles facilitate the isolation of highly pure lysosomal preparations from EpH4 cells for mass-spectrometry analysis

We previously developed a magnetic iron nanoparticle protocol to isolate functional lysosomes for membrane permeability studies²⁰. To investigate the suitability of these preparations

Stat3 alters proteins in the lysosomal membrane

for downstream MS analysis we sought to further characterise the lysosomes isolated using this method. By transmission electron microscopy (TEM) we observed that fluid phase uptake of nanoparticles by EpH4 cells led to the specific loading of degradative lysosomal vacuoles (Fig. 1A). Importantly, these particles were non-toxic, and cytotoxicity was only observed in the presence of hydrogen peroxide (Fig. 1B), likely a consequence of reactive free radicals generated by the Fenton reaction³². Using iron nanoparticles we were able to enrich and isolate EpH4 lysosomes with relative ease (Fig. 1C). The lysosomal identity of the isolated organelles was confirmed by TEM analysis, which showed the presence of vacuolar structures containing magnetic nanoparticles (Fig. 1D, top panel). Furthermore, negative staining of samples also revealed the presence of iron-containing membrane bound organelles that were the size and morphology consistent with lysosomes (Fig. 1D, lower panel). Importantly, fluorescence imaging and western blot analysis of iron-labelled (Mag+) preparations revealed near-undetectable levels of mitochondrial proteins (Fig. 1E and F), a common contaminant of lysosomal preparations isolated using methods such as density gradient centrifugation. In addition, contamination by other organelles, including endocytic vesicles and endoplasmic reticulum (ER), was minimal (Fig. 1F), demonstrating the effectiveness of this method for yielding highly pure lysosomal preparations.

To further enrich for lysosomal membrane proteins, and to reduce the contribution from cargo delivered to the lysosomes for degradation, isolated preparations were subjected to hypotonic lysis and centrifugation to separate lysosomal membranes. Using this method, the lysosomal membrane protein LAMP2 could be specifically detected in membrane fractions (LM, Fig. 2A). However, the lysosomal hydrolase cathepsin L (Ctsl) was detected at comparable levels in both membrane (LM) and soluble compartments (LC) of purified lysosomes (Fig. 2A and B), suggesting that not all organelles were successfully ruptured. To overcome this potential issue, preparations were subsequently subjected to repeat cycles of freeze-thawing. This optimisation improved the enrichment of cathepsin activity in the soluble fraction (Fig. 2C), indicating the enhanced disruption of lysosomes. We also assessed the activity of β -glucuronidase, a lysosomal enzyme that is predominately localised in the lysosomal

matrix and has minimal adherence to membranes³³, to more definitively assess the degree of lysosomal membrane disruption. As expected, β -glucuronidase activity in the soluble fraction was higher than in membrane preparations, and was markedly increased by freeze thawing (Fig. 2D). Therefore, hypotonic lysis of isolated lysosomes, combined with freeze fracture, facilitated the enrichment of lysosomal membranes for downstream MS analysis.

Mass-spectrometry analysis of EpH4 cell lysosomal membrane preparations isolated using iron nanoparticles

To further validate and assess the efficacy of the optimised lysosomal membrane isolation procedure prior to undertaking large scale experiments, a pilot preparation was submitted for LC-MS/MS analysis. Here, 1664 proteins were identified by MS (Supplementary Table S1A), which notably included numerous known lysosomal membrane proteins^{8,34} (Table 1), thus validating the utility of our lysosomal purification method for downstream proteomic analysis. Proteins that were also identified in the corresponding unlabelled (no magnetic particles) control sample (327 proteins, Supplementary Table S1B), and that did not belong to the endocytic-lysosomal pathway, were removed from this list. Furthermore, published common contaminants of MS experiments³⁵, such as heat shock proteins, keratins, tubulins, actins, elongation factors, histones, ribosomal and ribonucleo-proteins, were also removed. This resulted in a subset of 1295 proteins (Supplementary Table S2). To obtain a functional overview of the proteins identified, Kyoto Encyclopedia of Genes and Genomes (KEGG) pathway and Gene Ontology (GO) enrichment analysis was undertaken using the online gene list enrichment analysis tool, Enrichr^{36,37} (<http://amp.pharm.mssm.edu/Enrichr/>). Analysis of the KEGG pathway annotations associated with this subset revealed a significant enrichment in proteins involved in lysosomal and related pathways, including neurodegenerative diseases allied with lysosomal dysfunction (Supplementary Fig. S1A and Supplementary Table S3A). Furthermore, GO term distribution analysis for Cellular Component (CC) confirmed the lysosomal and vesicular membrane localisation of the identified proteins (Supplementary Fig. S1B and Supplementary Table S3B). Functional analysis also revealed the enrichment of mitochondrial membrane proteins

Stat3 alters proteins in the lysosomal membrane

involved in oxidative phosphorylation (Supplementary Fig. S1A and B). This suggests that lysosomal preparations isolated using iron nanoparticles may contain a degree of mitochondrial contamination that is undetectable by western blotting or MitoTracker™ analysis (e.g. Fig. 1E, F). However, it is important to note that this contamination may also reflect the delivery of damaged mitochondria to the lysosome for turnover during mitophagy^{20,38}, or the remnants of lysosome-mitochondrial contact sites^{39,40}.

Oncostatin M stimulates vesicle biogenesis in EpH4 cells

We have previously shown that stimulation of EpH4 mammary epithelial cells by OSM leads to LMP³⁰. OSM-induced Stat3 phosphorylation in EpH4 cells resulted in the increased expression of multiple target genes, including the PI3Kinase subunits p55 α and p50 α ⁴¹ and the lysosomal protease cathepsin B (Ctsb, Fig. 3A), alongside increased vacuole formation (Fig. 3B)²⁰, which appeared to be degradative in nature (Fig. 3C). These structures accumulate the lysosomotropic dye LysoTracker® Red, thus revealing their lysosomal origin (Fig. 3D). Notably, the apparent size of the lysosomal compartment is increased by OSM treatment, and is associated with a more perinuclear localisation (Fig. 3D).

To further characterise Stat3 induced changes to the lysosomal compartment, we sought to isolate lysosomes from OSM stimulated EpH4 cells using the optimised magnetic nanoparticle fractionation protocol. Western blot analysis of the lysosomal markers LAMP2 and cathepsin L (Ctsl) demonstrated that this technique was also applicable to OSM treated cells, and that the stimulation did not significantly interfere with iron uptake (Fig. 3E). Interestingly, OSM treatment resulted in increased LAMP2 glycosylation, as observed by the molecular weight shift in LAMP2 on western blot (Fig. 3E). Prolonged OSM treatment resulted in cell death (Fig. 3B)³⁰, leading to a reduction in protein yields as compared to control treated EpH4 cells (PNS lane in Fig. 3E). Despite this, OSM mediated induction of cathepsin L expression corresponded to an approximately sixteen-fold increase in enzyme activity inside the lysosomal matrix (LC, Fig. 3F).

OSM induced changes to the EpH4 lysosomal proteome

Having established that lysosomes from OSM treated EpH4 cells could be isolated using our purification method, we then investigated the effect of Stat3 activation on the lysosomal proteome. Lysosome membrane preparations from three independent biological replicates of vehicle and OSM treated cells were submitted for LC-MS/MS analysis. For each replicate a corresponding unlabelled (no iron particles) control was also included to filter out non-specific contaminants. Prior to MS analysis, lysosomes purified from OSM and control (vehicle) treated cells were assessed for lysosomal membrane enrichment (Fig. 4A) and purity (Fig. 4B). Importantly, western blot analysis of iron-labelled lysosomal membrane (LM) preparations revealed near-undetectable levels of contamination by other organelles (Fig. 4B). However, we observed low levels of COX IV, a mitochondrial marker, in one of the three replicates (Fig. 4B), which was either derived from contaminating mitochondria or from lysosomal mitophagic cargo. A label-free, emPAI-based semi-quantitative proteomics approach was used to profile OSM induced changes in protein abundance (see methods). Raw data for all samples are shown in Supplementary Table S4. MS analysis of three independent biological repeats (three OSM and corresponding vehicle control samples) resulted in the identification of 35076 spectra within a 1% false discovery rate (0.66% decoy FDR), and an average spectrum identification rate of over 24% (Supplementary Table S5). Coalescence of redundant identifications from repeat and overlapping peptides resulted in a list of 644 unique proteins at a probability of over 99%, which contained at least 3 identified peptides (established at greater than 95% probability), within a false discovery rate of less than 5% (Fig. 4C, Supplementary Tables S4 and S6). Proteins that were also identified in the corresponding unlabelled (no magnetic particles) control sample for each independent replicate, and not belonging to the endocytic-lysosomal pathway, were removed from this list. In addition, known common contaminants³⁵ were deleted as before. Exceptions to this rule were considered if their representations changed significantly with OSM treatment; e.g. Keratin 8, which is a definitive marker of luminal mammary epithelial cells. This resulted in a subset of 447 proteins (Fig. 4C and Supplementary Table S7). 320 out of 447 were identified in at least 5 of the 6 preparations (3 x vehicle, 3 x OSM treated samples)

Stat3 alters proteins in the lysosomal membrane

(Supplementary Table S8). Pathway analysis (KEGG, 2016) on this more stringent subset validated the lysosomal nature of the proteins identified, which included numerous known lysosomal components (Fig. 4D and Supplementary Table S9A). A significant enrichment was also observed for components involved in phagocytosis. This is not unexpected given the ultimate destination of phagosomes is the lysosomal compartment. Moreover, GO term distribution analysis for Cellular Component (CC) confirmed the lysosomal and vesicular membrane localisation of the identified proteins (Fig. 4E and Supplementary Table S9B). In vehicle and OSM treated samples, three and 21 proteins were exclusively identified, respectively (Fig. 4C, Table 2).

Whilst the lysosomal nature of most proteins (408/447) remained similar between vehicle and OSM treated preparations, a subset of 39 proteins (~ 9%) showed more significant changes in abundance between the different conditions (Fig. 4C, Table 3 and Supplementary Table S10). A striking decrease in lysosomal enzymes, including galactocerebrosidase, beta-hexosaminidase and lysosomal alpha-mannosidase was observed with OSM treatment (Fig. 4F, Table 3 and Supplementary Table S10), suggesting either that Stat3 affects the distribution of these enzymes or, more likely, that these have been depleted from the lysosomes as a result of LMP. OSM stimulation also resulted in the increased representation of cell surface proteins and cytoskeletal components such as integrins, annexins and flotillins (Fig. 4F, Table 3 and Supplementary Table S10). Interestingly, this suggests that endocytosis, and the subsequent transport and localisation of cargo into the lysosomal compartment, is stimulated upon Stat3 activation, supporting our previous observations *in vivo*²⁰.

In order to validate these results, immunoblot analysis of lysosomal protein preparations, used for the MS analysis, was undertaken. Flotillins are interesting candidates as they are involved in endocytosis and membrane trafficking, and form clusters in plasma membrane lipid rafts^{42,43}. Flotillin 1 was significantly enriched in lysosomes isolated from OSM stimulated cells (Fig. 4F, Table 3) and whilst not statistically significant, the related protein flotillin 2 also showed an increased representation in OSM treated lysosomes (Fig. 4F). While flotillin 1 and flotillin 2 were undetectable in lysosomal preparations from

untreated EpH4 cells, OSM stimulation of Stat3 activity resulted in the appearance of considerable amounts of both these proteins in the lysosomal compartment (Fig. 5A). This is not surprising as flotillin 2 has previously been observed to traffic from the plasma membrane to endosomes^{42,43}, which may subsequently fuse with lysosomal structures. Further support for the endocytosis of flotillins in response to Stat3 is provided by the observation that OSM treatment of EpH4 cells for only 24h resulted in increased internalisation of flotillin 2 puncta in EpH4 cells (Supplementary Fig. S2).

Annexins A1, A6 and A11 were also enriched in lysosomal fractions following OSM stimulation (Table 3). Our previous microarray data of a mammary gland developmental cycle⁴⁴ revealed the downregulation of these annexins during lactation (Supplementary Fig. S3). Interestingly, while expression levels of annexin A6 remained fairly consistent across all lactation and involution timepoints, a substantial increase in the expression of annexins A11 and A1 was observed during involution (Supplementary Fig. S3). This pattern is similar to that of flotillins 1 and 2 (Fig. 5B) suggesting that all these membrane proteins may play significant roles in regression of the mammary gland. Indeed, mRNA expression of both *Flot1* and *Flot2* is downregulated approximately 2-fold in the mammary glands of Stat3 knock-out mice at 24 h involution (Supplementary Table S11). In addition, the glutathione-S-transferase *Mgst1* was also identified in lysosomal preparations purified from OSM-treated EpH4 cells (Tables 2 and 3). *Mgst1* is a de-toxifying enzyme and therefore may be upregulated in response to iron nanoparticle uptake. However, as it is only present in the OSM treated samples, it is tempting to speculate that it could be induced to protect against the effects of LMP. Indeed, an increase in *Mgst1* and the related protein *Mgst3* is observed during mammary gland involution (Supplementary Fig. S3), suggesting that they may possess important functions during lysosomal-mediated cell death *in vivo*.

Whilst a significant number of known lysosomal membrane proteins were identified by MS analysis, the relative yield of some peptides (including from abundant proteins such as LAMP1 and 2) was lower than expected, similarly to that observed in previous studies³⁴. One possible explanation is that the heavily glycosylated nature of many lysosomal membrane proteins may interfere with MS

Stat3 alters proteins in the lysosomal membrane

analysis. To address this possibility, lysosomal membrane samples were deglycosylated using Peptide-N-Glycosidase F (PNGase F) prior to proteomic analysis. PNGase F is an amidase that cleaves between the innermost N-Acetylglucosamine (GlcNAc) and asparagine residues of oligosaccharides from N-linked glycoproteins⁴⁵. PNGase F treatment resulted in the efficient removal of N-linked glycans from LAMP2 proteins, as shown by the appearance of a sharp band at approximately 30 kDa by immunoblot analysis (Supplementary Fig. S4). To determine whether the representation of heavily glycosylated proteins is improved after deglycosylation, PNGase F-enzyme treated and untreated lysosomal membrane samples were analysed by LC-MS/MS. Western blot analysis of various organelle markers was performed to check the purity of the preparations as described before (Supplementary Fig. S4). 955 and 718 proteins were identified in control and enzyme-treated lysosomal membrane samples respectively (Supplementary Table S12). Comparative analysis of heavily glycosylated proteins, such as LAMP1, LAMP2, LIMP2 and CD63/LIMP1, revealed that deglycosylation increased the number of unique peptide sequences identified for these proteins, vastly improving their representation and identification by LC-MS/MS (Supplementary Table S13). Of note, deglycosylation did not appear to have a detrimental impact on the identification of lysosomal membrane proteins, with the majority higher ranked in PNGase F-treated samples (Supplementary Table S13). Therefore, future proteomic experiments investigating lysosomal membrane composition will likely benefit from utilising deglycosylating approaches prior to LC-MS/MS.

Stat3 mediated regulation of the lysosomal compartment

To investigate the biological relevance of OSM-induced changes to the lysosomal compartment, we used CRISPR/Cas9 technology to ablate Stat3 in EpH4 cells. Mass spectrometry analysis revealed that the lysosomal membrane protein LAMP2 is upregulated in response to OSM stimulation of Stat3 activity (Fig. 4F, Table 3). Indeed, LAMP2 and LAMP1 immunostaining in EpH4 cells clearly showed enhanced lysosomal biogenesis in response to OSM, with lysosomes becoming increasingly perinuclear in distribution (Fig. 5C). Surprisingly, we found that deletion of Stat3 abrogated the increase in apparent

molecular weight of LAMP1 and LAMP2 that occurs in response to OSM treatment (Figs. 3E and 5D) suggesting a role for this post-translation modification of LAMP1 and LAMP2 in lysosome function. Importantly, a similar shift in mobility is observed during involution of the mouse mammary gland³⁰, and is likely due to a change in glycosylation. Stat3 also upregulates expression of the lysosomal protease cathepsin B and the endo-lysosomal membrane protein, CD63 (Fig. 5D and Supplementary Table S11). At a transcriptional level, both *CD63* and *Lamp2* mRNAs are downregulated during lactation, and rise sharply during involution (Fig. 5E). Together, these data suggest that Stat3 directly modulates lysosomal membrane constituents to induce lysosomal leakiness and consequent cell death.

Discussion

The lysosome is enjoying a renaissance as a signalling centre and monitor of cellular nutritional status⁴⁶. While microarray studies are very useful in highlighting transcriptional changes in response to transcription factors such as Stat3, these are of little value in determining the functional downstream consequences of altered protein expression. Having determined a role for Stat3 in lysosomal function, we aimed to characterise this at the level of the lysosomal membrane proteome in order to shed further light on the mechanism of LMP in mammary epithelial cells.

In the past decade, an increased knowledge of the lysosomal proteome has been acquired through the application of MS^{8,14,22,34}. However, although numerous lysosomal membrane proteins have so far been identified using density centrifugation^{14,34}, these data do not fully correlate with the plethora of known and crucial functions of the lysosomal membrane and its constituent proteins and enzymes. This failure to detect all lysosomal membrane proteins, coupled with the contamination inherent in lysosome enrichment approaches used to date, prompted us to develop an alternative method to enrich lysosomal membrane proteins. In order to circumvent alterations in the size or buoyant density of lysosomes in response to changes in cellular status, we utilised a different approach that is independent of these features. Labelling and subsequent isolation of lysosomes by uptake of magnetic nanoparticles resulted in highly pure lysosomal membrane preparations being obtained. Although proteins that reside in other

Stat3 alters proteins in the lysosomal membrane

organelles were not detected by immunoblotting and MitoTrackerTM analysis, a number of mitochondrial and other organellar proteins were detected by MS. Although this could be due to contamination, we suggest it is more likely the consequence of autophagy, which we have previously shown to be induced in Eph4 cells, particularly in response to OSM³⁸. Indeed, we observed a considerable number of degradative structures present even in control, non-OSM stimulated cells (Fig. 3)²⁰. Functional analysis of our MS data corroborated the lysosomal nature of the samples, and provided valuable insights into membrane trafficking events as well as lysosomal function. Importantly, although heavily glycosylated proteins such as LAMP1, LAMP2, CD63/LIMP1 and LIMP2 were detected, they were relatively underrepresented. This is likely due to glycosylation-mediated changes in mass and therefore the time of flight, which has an impact on the resolution of the peptide spectrum acquired⁴⁷. We show that prior deglycosylation treatment considerably improves the representation of these proteins (Supplementary Table S13), and suggest that future proteomics experiments should consider utilising this approach.

We analysed the lysosomal proteome in both intact and leaky lysosomes, the latter treated with OSM to induce Stat3 activation and subsequent LMP. Interestingly, OSM treatment resulted in a clear loss of lysosomal enzymes, probably as a consequence of LMP and leakage of proteases to the cytosol. In contrast, OSM induced elevated levels of cargo probably as a consequence of increased endocytosis and downregulation of cell surface receptors and adhesion complexes that are subsequently delivered to the lysosome. Observed changes in cytoskeletal proteins may be relevant to lysosomal localisation, which in turn influences internal pH⁴⁸ with possible effects on protease functions and LMP. In support of this notion, OSM stimulation intriguingly resulted in increased perinuclear distribution of lysosomes in Eph4 cells (Figs. 3D and 5C).

Interesting candidates for further characterisation include flotillins 1 and 2. Data from this study show that OSM treatment causes trafficking of these proteins to the degradative endo-lysosomal pathway. Flotillins (or reggies) form clusters in lipid rafts, and have been shown to regulate trafficking of $\alpha 5$ and $\beta 1$ integrins and thus the formation of focal adhesions⁴⁹. We speculate that OSM treatment induces cells to

detach with consequent turnover of focal adhesions and trafficking of integrins to the lysosome. Indeed, mRNA expression of both *Flot1* and *Flot2* is downregulated approximately 2-fold in the mammary glands of Stat3 knock-out mice at 24 h involution (Supplementary Table S11). Their roles in regulating mammary cell death during involution *in vivo*, therefore, warrants further investigation.

Other interesting candidates for validation include annexins A1 (Anxa1), A6 (Anxa6) and A11 (Anxa11). Annexins are a family of highly conserved proteins that bind to negatively charged phospholipids and membranes in a calcium dependent manner⁵⁰. Studies in annexin knockout mice have suggested that annexin-A1 fulfils multiple roles, including trafficking at the plasma membrane and in the endocytic compartment⁵⁰. Annexin-A6 is also involved in membrane organisation and the distribution of proteins in rafts⁵¹. Recently, annexin-A11 has been shown to physically associate with a component of the coat protein complex II (COPII) machinery that is associated with the ER and controls transport of transmembrane cargoes from the ER to the Golgi⁵². Thus, the changes we have observed in lysosomal levels of these three annexins could be a reflection of the elevated vesicle formation induced by OSM.

Finally, using CRISPR/Cas9 technology to ablate Stat3 in Eph4 cells, we reveal a direct role for Stat3 signalling in the regulation of lysosomal proteins such as cathepsin B, CD63, LAMP1 and LAMP2. Surprisingly, we show that Stat3 regulates the glycosylation status of LAMP1 and LAMP2 in response to OSM treatment in Eph4 cells (Fig. 5D), mimicking that observed during involution of the mouse mammary gland³⁰. An intriguing possibility is that Stat3 could induce expression of fucosyltransferases in mammary epithelial cells, since LIF/Stat3 has been shown to regulate expression of alpha1,2-fucosyltransferases FUT1 and FUT2, which transfer fucoses onto the terminal galactose of N-acetyl-lactosamine⁵³. It has been shown recently that FUT1 regulates the subcellular localisation of lysosomes, with FUT1 knockdown inducing perinuclear accumulation⁵⁴, similar to that observed upon OSM stimulation (Figs. 3D and 5C). Together, our data suggest that Stat3 activation induces endocytosis of plasma membrane constituents (including flotillins and annexins) that consequently results in a dramatic increase in endo-lysosomal trafficking, and the

Stat3 alters proteins in the lysosomal membrane

subsequent enhancement of the lysosomal system.

In summary, this study has refined the utility of magnetic iron nanoparticles for the isolation of highly pure lysosomal membrane preparations for downstream proteomic analysis. Notably, this method can be applied to purify leaky lysosomes undergoing membrane permeabilisation, revealing valuable insights into the cellular trafficking events that may contribute to Stat3-mediated cell death. Vacuolisation is implicated in driving cell death in a variety of organisms, including plant⁵⁵ and *Dictyostelium discoideum*⁵⁶ cells. Intriguingly, an activated form of the H-Ras oncoprotein was recently reported to induce extensive vacuolisation and subsequent cell death in cultured cancer cells⁵⁷. Thus, our method may be utilised more widely to investigate the lysosomal proteome in contexts associated with lysosomal perturbations, such as cancer, neurodegenerative diseases and lysosomal storage disorders. An improved understanding of the mechanisms driving lysosomal membrane permeabilisation is pivotal for developing new and effective therapies against the many disorders associated with aberrant lysosomal function.

Experimental procedures

Cell Culture

EpH4 cells⁵⁸ were maintained in DMEM (Life Technologies) media supplemented with 10% FCS (Sigma) at 37 °C in a humidified atmosphere of 5% CO₂. For OSM stimulation, cells were stimulated at 50% confluency with a final concentration of 25 ng ml⁻¹ recombinant mouse oncostatin M (495-MO, R&D Systems) or carrier (0.0001% BSA in PBS) in DMEM supplemented with 1% FCS. Medium was renewed with fresh OSM (in 1% FCS/DMEM) after 48 h. Cells were harvested 72 h after stimulation. Cytotoxicity was assessed by trypan blue exclusion.

CRISPR/Cas9 Stat3 KO cell line generation

Two SpCas9 guide sequences targeting the mouse Stat3 gene were designed using the sgRNA scoring algorithm from Doench and colleagues⁵⁹. These were cloned into the lentiCRISPRv2 plasmid, lentivirus was produced, EpH4 cells were transduced and puromycin selected according to previously described protocols^{60,61}. Using these, two independent Stat3KO lines were derived and maintained in the

pooled state (as single cell cloning of EpH4 cells would likely lead to clonal artefacts). Stat3KO1 was created from virus expressing the guide sequence GTACAGCGACAGCTTCCCA, and Stat3KO2 from virus expressing the guide sequence GGAAGTCCGCAGCTCCATG. As these two lines use different guide sequences, they act as off-target controls for one another and so any phenotypes observed can be attributed to the loss of Stat3. Deletion of Stat3 was confirmed by TIDE analysis⁶² and western blotting. To further control for any effects of lentiviral transduction and SpCas9 expression, virus expressing a 'scrambled' guide (AAATTAATTTAATTTAAAG) that does not target any mouse coding sequences was also used.

Ferrofluid labelling and purification of lysosomes

Lysosomes from EpH4 cells were purified using magnetic iron nanoparticles (EMG-508, Ferrotec) as previously described²⁰. Briefly, EpH4 cells were seeded at a density of 3×10⁶, or 1×10⁶ for OSM stimulation, in 15 cm tissue culture plates (168381, Nunc). The following day, or after 48 h of OSM stimulation, cells were labelled for 4 h in iron nanoparticle containing media (EMG series 508, FerroTec, 1:100) followed by a 20 h chase period in clean media (including fresh OSM in the case of stimulation experiments). Cells were then scraped in PBS, pelleted in a table-top centrifuge (300 r.p.m., 4°C, 3 min) and the pellet homogenised in a tight-fitting handheld homogenizer (5 strokes) in 700 µl subcellular fractionation buffer (HEPES-KOH 20 mM, sucrose 250 mM, KCl 10 mM, MgCl₂ 1.5 mM, EDTA 1 mM, EGTA 1 mM, dithiothreitol 8 mM, Complete protease inhibitor (Roche) at pH 7.5). The homogenate was spun at 750 g (3,500 r.p.m., 4°C, 10 min) to remove nuclei and other debris, followed by a second 750 g spin to ensure complete removal of contaminating heavy membranes. The resulting supernatant (PNS; post nuclear supernatant) was transferred into a clean tube, loaded onto a magnetic rack and incubated for 1 h at 4°C on a rocker. A 50 µl sample of PNS was retained for analysis. Following incubation tubes were left on the magnet and the supernatant (SN) removed (retaining 50 µl for analysis). Tubes were washed three times with 1 ml of subcellular fractionation buffer. Following addition of the last wash tubes were removed from the magnet, and spun at 12,000 r.p.m. (13,800 g, 4°C, 15 min) to pellet magnetite-containing lysosomes. To limit

Stat3 alters proteins in the lysosomal membrane

contamination by proteins non-specifically sticking to the eppendorf pellets were resuspended and combined in a final volume of 200 μ l fractionation buffer and transferred into a clean eppendorf. The samples were then pelleted at 13,800 g for a further 15 min at 4 °C, along with the PNS and SN samples.

Fractionation of purified lysosomes

To obtain “total” lysosomal lysates, whole lysosomes purified as described above were incubated with 0.1% Triton X-100 (VWR) for 10 min on ice, intermittently vortexed four times and spun at 12,000 r.p.m (13,800 g, 4°C) for 15 min. The supernatant was transferred into new tubes. To separate the lysosomal content from the lysosomal membrane fraction, the isolated lysosomes were resuspended in 5 mM Tris buffer pH 7.5, incubated on ice for 30 min or frozen in liquid nitrogen, and thawed at 37°C five times. Lysosomal membranes were pelleted by spinning at 15,000 g for 30 min at 4°C. The supernatant (lysosomal content, LC) was transferred into a new tube. The pellet was resuspended in 50 μ l 0.1% Triton X-100 in PBS, incubated 10 min on ice and intermittently vortexed four times. After spinning at 17,000 g for 10 min at 4°C the supernatant (lysosomal membrane fraction, LM) was transferred into fresh tubes.

Immunoblotting

PNS and SN samples were pelleted and resuspended in 50 μ l modified RIPA buffer (50 mM Tris, 1% NP40, 0.25% sodium deoxycholate, 150 mM NaCl, 1 mM EGTA and complete protease inhibitor), and lysed on ice for 30 min with intermittent vortexing. Samples were then spun at 12,000 r.p.m. (13,800 g, 4°C, 15 min) and the supernatant retained for western blotting analysis. Protein samples (made up in modified RIPA buffer, 0.1% Triton X-100 or 5 mM Tris as described above) were denatured and resolved on SDS–polyacrylamide gels. Proteins were separated by SDS-PAGE under reducing conditions unless otherwise stated. Immunoblotting was performed using standard techniques and antibody detection was achieved with enhanced chemiluminescence reagent (ECL, GE Healthcare). The following primary antibodies were used: rat anti-LAMP2 (ab13524, Abcam, 1:1,000), goat anti-cathepsin L (AF1515, R&D Systems, 1:1,000), goat anti-cathepsin B (AF965, R&D Systems, 1:1,000), mouse anti-COX IV (ab33985, Abcam, 1:1,000), rabbit anti-

PI3 Kinase, p85 (06-496, Millipore, 1:1000), rabbit anti-Stat3 (sc-482, Santa Cruz, 1:1000), rabbit anti-phospho Stat3 (9131, Cell Signaling, 1:1000), mouse anti-ERp57 (sc-23886, Santa Cruz, 1:400), rabbit anti-GAPDH (5174, Cell Signaling, 1:1000), goat anti-histone H3 (sc-8654, Santa Cruz, 1:1000), rabbit anti-Rab5 (2143, Cell Signaling, 1:1000), rat anti-LAMP1 (ID4B, Developmental Studies Hybridoma Bank 1:200), rat anti-CD63 (NVG-2 #143901 Biologend, 1:1000), rabbit anti-flotillin 1 (#18634 Cell Signaling Technology 1:800) and rabbit anti-flotillin 2 (HPA0013961, Atlas Antibodies 1:200). All horseradish peroxidase (HRP)-conjugated secondary antibodies were from Dako.

Cathepsin Activity Assay

10 μ l of lysates were added to a total of 200 μ l cathepsin reaction buffer (sodium acetate 50 mM, EDTA 8 mM, dithiothreitol 8 mM and Pefabloc subcellular fractionation buffer 1 mM, at pH 6). Cathepsin B and L activity was measured with the fluorescent substrate Z-Phe-Arg-AMC (50 μ M; Merk Millipore) in a Synergy HT Multi-Detection Microplate Reader (excitation 380 nm, emission 442 nm; Bio-TEK). Fluorescence was measured immediately every minute for 1 h at 37°C. Initial rates of cathepsin B and L activity were determined from the linear part of the resulting curve and normalized to total cathepsin activity obtained from Triton X-100-extracted lysates. Cathepsin activity reaction buffer alone or containing 50 μ M z-F-R-AMC served as controls. The assay was performed in duplicate or triplicate per condition in a 96-well flat bottom microtitre plate (Thermo Scientific).

β -glucuronidase Assay

10 μ l of lysates were added to 125 μ l of Sodium Acetate/Acetic Acid Buffer (0.1 M sodium acetate, 0.1 M acetic acid, pH 4.8) containing 10 mM of the fluorescent substrate 4-Methylumbelliferone- β -D-glucuronide (4-MU-Glu, Biosynth) on ice. Samples were incubated for 30 min at 37°C, and the reaction subsequently stopped by the addition of 100 μ l Glycine/Carbonate Buffer (0.17 M glycine, 0.17 M sodium carbonate, pH 9.8) on ice. Fluorescence was measured in a Synergy HT Multi-Detection Microplate Reader (excitation 380 nm, emission 442 nm; Bio-TEK). Sodium Acetate/Acetic Acid Buffer alone or containing 10 mM 4-MU-Glu served as controls. The assay was performed in duplicate or triplicate per

Stat3 alters proteins in the lysosomal membrane

condition in a 96-well flat bottom microtitre plate (Thermo Scientific).

FITC dextran and mitotracker staining of lysosomal preparations

EpH4 cells were seeded at a density of 3×10^6 in 15 cm Nunc cell culture dishes (Thermo Scientific). Plates were either labelled for 2 h with 2.5 mg/ml 10 kDa FITC-dextran (Sigma) in 10% DMEM containing 10% Ferrofluid in BSA/PBS (+) or in FITC-dextran containing media only (minus iron nanoparticles (-)). Cells were washed three times in PBS followed by a 2 h chase period in 10% DMEM, prior to labelling of mitochondria with 500 nM Mitotracker (MitoTracker Red FM, Invitrogen) in 10% DMEM for 30 min. Plates were then washed three times in PBS and the cells scraped into 500 μ l PBS and spun at 900 g for 3 min at 4°C. Cell pellets were resuspended in 700 μ l fractionation buffer containing complete protease inhibitors and homogenised with five strokes in a dounce homogenizer. To obtain the PNS the homogenate was spun at 800 g for 10 min at 4°C. The PNS was transferred into a new tube and 50 μ l retained for analysis (PNS -/+). The PNS was incubated on a magnetic rack for 1 h at 4°C on a rocker. Post incubation the supernatant (SN) was removed and 50 μ l kept for analysis (SN -/+). The tubes were washed three times with 1 ml cold fractionation buffer on the magnetic rack. Following the last wash, the tubes were removed and spun at 13,800 g for 15 min at 4°C. The lysosomal pellet (LP -/+) was resuspended in 25 μ l fractionation buffer. 10 μ l of the magnetic nanoparticle labelled and unlabelled PNS, SN, and lysosomal pellets were mixed with 10 μ l PBS/glycerol (v/v 50:50) and dropped onto a microscope slide and covered by a cover slip for imaging using a Zeiss Axioplan 2 microscope and a Plan-APOCHROMAT 63x/1,4 oil objective (Zeiss).

Immunofluorescence and LysoTracker Red staining

EpH4 cells were seeded on glass coverslips or ibidi 35mm glass bottom dishes and stimulated with OSM as described above the following day. After OSM stimulation cells were fixed with 4% paraformaldehyde for 5 min at 37°C and subsequently permeabilized with 0.5% v/v TritonX-100 in PBS for 10 min at room temperature. Cells were blocked in 10% normal goat serum (Sigma) in PBS for 1 h at room temperature and then incubated with primary antibody in PBS for 1 h at room temperature, or

overnight at 4°C. Primary antibodies used were rat anti-LAMP2 (GL2A7 #ab13524, Abcam 1:200), rat anti-LAMP1 (ID4B, Developmental Studies Hybridoma Bank 1:200) and rabbit anti-flotillin 2 (HPA0013961, Atlas Antibodies 1:200). Cells were then washed in PBS followed by secondary antibody staining (Cy3 goat anti-rat IgG, Life Technologies, 1:500; Alexa Fluor 488 goat anti-rabbit IgG, Invitrogen A11008, 1:500; or Alexa Fluor 647 goat anti-rat IgG, Life Technologies A21247, 1:500) for 1 h at room temperature. Nuclei were counterstained with Hoechst 33342 (Sigma Aldrich; 1:1000). Cells were stained with LysoTracker Red DND-99 (Life Technologies) at 1:10,000 for 30 min at room temperature according to manufacturer's instructions. Images were acquired using a Zeiss Axioplan 2 microscope (Zeiss, Jena, Germany) or a Leica TCS SP8 inverted confocal microscope. Image reconstructions were generated ImageJ (v1.50c, National Institutes of Health)⁶³.

Transmission electron microscopy (TEM)

EpH4 cell lysosomes were isolated using the magnetic nanoparticle protocol and adsorbed to a TEM grid. This was followed by two wash steps in H₂O to remove any remaining buffer salts. Samples were either directly imaged using a Tecnai G2 electron microscope or negatively stained with 1% uranyl acetate beforehand.

Silver staining of protein gels

Protein samples were run on 4-15% Mini-Protean TGX Gels (BioRad) and fixed in 45% methanol, 1% v/v in ddH₂O for 30 min. After washing in ddH₂O the gels were sensitized with 0.02% sodium thiosulfate (Na₂S₂O₃) for 1 min and rinsed in ddH₂O three times for 20 sec. Afterwards the gels were stained in ddH₂O containing 0.2% silver nitrate (AgNO₃) and 0.02% Formaldehyde for 20 min. This was followed by rinsing two times in ddH₂O for 20 sec and developing for 3 min in 3% sodium carbonate (Na₂CO₃), 0.0005% sodium thiosulfate, 0.05% Formaldehyde in ddH₂O. The developed gels were rinsed two times in ddH₂O for 20 sec and blocked in 5% Acetic Acid.

Mass-spectrometry methods

All MS experiments were undertaken at the Cambridge Centre for Proteomics (University of Cambridge). For all experiments submitted for MS analysis, a corresponding unlabelled (no magnetic particles) control sample was also analysed. For the OSM-related experiments, three

Stat3 alters proteins in the lysosomal membrane

independent biological repeats (three OSM and corresponding vehicle control samples) were performed, and a corresponding unlabelled (no magnetic particles) control sample also submitted for each independent replicate.

Silver destaining and tryptic digest

After 1D gel electrophoresis, gel pieces were cut into 1-2 mm cubes and placed into 0.5 ml tubes. The gel pieces were incubated with 100 μ l silver destaining solution (a 1:1 ratio of 27 mM potassium ferricyanide ($K_3[Fe(CN)_6]$) and 100 mM sodium thiosulphate ($Na_2S_2O_3$) in high performance liquid chromatography (HPLC) grade water) for 10 min at 37°C. This step was repeated with fresh destaining solution until complete clarification of the gel pieces. Subsequently, pieces were washed in HPLC grade water, prior to incubation in 100% acetonitrile at 37°C until they appeared white and shrunken. The acetonitrile was removed and any residual solution evaporated by incubating at 37°C for 10 min. To reduce the proteins, the gel pieces were incubated in 50 μ l 10 mM DTT made up in 100 mM ammonium bicarbonate (NH_4HCO_3) at 56°C for 1 h. For alkylation 50 μ l 55 mM iodoacetamide (C_2H_4INO) made up in 100 mM ammonium bicarbonate was then added, and incubated at room temperature in the dark for 45 min. The liquid was removed and 100 μ l 100 mM ammonium bicarbonate added and incubated at 37°C for 10 min. After removing the liquid, the gel pieces were incubated in 50% acetonitrile (C_2H_3N) in 100 mM ammonium bicarbonate at 37°C for 10 min, which was then replaced by 100 μ l 100% acetonitrile to dry the gel pieces. To evaporate the acetonitrile, the gel pieces were incubated further at 37°C, to ensure that they were completely dry prior to tryptic digest. 50-60 μ l of trypsin solution (10 ng/ μ l in 50 mM ammonium bicarbonate) was added to the gel pieces and incubated overnight.

LC-MS/MS analysis

After tryptic digestion, the supernatant was pipetted into a sample vial and loaded onto an autosampler for automated LC-MS/MS analysis. The pilot LC-MS/MS experiment was performed using a Dionex Ultimate 3000 RSLC nanoUPLC (Thermo Fisher Scientific Inc, Waltham, MA, USA) system and a QExactive Orbitrap mass spectrometer (Thermo Fisher Scientific Inc, Waltham, MA, USA). All OSM-related and deglycosylation experiments were performed using a Waters NanoAcquity UPLC

(Thermo Fisher Scientific Inc, Waltham, MA, USA) system and an Orbitrap Velos mass spectrometer (Thermo Fisher Scientific Inc, Waltham, MA, USA). For the pilot experiment using the Q Exactive, separation of peptides was performed by reverse-phase chromatography at a flow rate of 300 nL/min and a reverse-phase nano Easy-spray column (Thermo Scientific PepMap C18, 2 μ m particle size, 100 Å pore size, 75 μ m i.d. x 50 cm length). Peptides were loaded onto a pre-column (Thermo Scientific PepMap 100 C18, 5 μ m particle size, 100 Å pore size, 300 μ m i.d. x 5mm length) from the Ultimate 3000 autosampler with 0.1% formic acid for 3 min at a flow rate of 10 μ L/min. After this period, the column valve was switched to allow elution of peptides from the pre-column onto the analytical column. Solvent A was water + 0.1% formic acid and solvent B was 80% acetonitrile, 20% water + 0.1% formic acid. The linear gradient employed was 2-40% B in 30 min. The LC eluant was sprayed into the mass spectrometer by means of an Easy-spray source (Thermo Fisher Scientific Inc.). All m/z values of eluting ions were measured in an Orbitrap mass analyzer, set at a resolution of 70000. Data dependent scans (Top 20) were employed to automatically isolate and generate fragment ions by higher energy collisional dissociation (HCD) in the quadrupole mass analyser and measurement of the resulting fragment ions was performed in the Orbitrap analyser, set at a resolution of 17500. Peptide ions with charge states of 2+ and above were selected for fragmentation.

For the nanoAcquity/Orbitrap Velos experiments, separation of peptides was performed by reverse-phase chromatography using a Waters reverse-phase nano column (BEH C18, 75 μ m i.d. x 250 mm, 1.7 μ m particle size) at flow rate of 300 nL/min. Peptides were initially loaded onto a pre-column (Waters UPLC Trap Symmetry C18, 180 μ m i.d x 20mm, 5 μ m particle size) from the nanoAcquity sample manager with 0.1% formic acid for 3 minutes at a flow rate of 10 μ L/min. After this period, the column valve was switched to allow the elution of peptides from the pre-column onto the analytical column. Solvent A was water + 0.1% formic acid and solvent B was acetonitrile + 0.1% formic acid. The linear gradient employed was 3-40% B in 40 minutes (60 minutes total run time including wash and equilibration steps).

The LC eluant was sprayed into the mass spectrometer by means of a standard Thermo Scientific nanospray source. All m/z values of

Stat3 alters proteins in the lysosomal membrane

eluting ions were measured in the Orbitrap Velos mass analyzer, set at a resolution of 30000. Data dependent scans (Top 20) were employed to automatically isolate and generate fragment ions by collision-induced dissociation in the linear ion trap, resulting in the generation of MS/MS spectra. Ions with charge states of 2+ and above were selected for fragmentation. Post-run, all data were processed using Protein Discoverer (version 2.1., ThermoFisher).

All LC-MS/MS data generated from the pilot and deglycosylation experiments were converted to mgf files and these files were then submitted to the Mascot search algorithm (Matrix Science, London UK) and searched against the Uniprot mouse database (UniProt_Mouse_Oct13_10090_Oct2013_82208 sequences; 36313543 residues) using a fixed modification of carbamidomethyl (C) and variable modifications of oxidation (M) and deamidation (NQ). Peptide identifications were accepted if they could be established at greater than 95.0% probability.

For analysis of OSM-related experiments data all MS/MS data were converted to mgf files and submitted to the Mascot search algorithm (Matrix Science, London UK) and searched against the swissprot_2013_11 database (with a mouse taxonomy filter, 16693 sequences). Mascot was searched with a fragment ion mass tolerance of 0.80 Da and a parent ion tolerance of 25 PPM. Trypsin was specified as the enzyme and carbamidomethyl of cysteine was specified in Mascot as a fixed modification. Deamidation of asparagine and glutamine and oxidation of methionine were specified in Mascot as variable modifications. For protein identification, Scaffold (version Scaffold_4.7.2, Proteome Software Inc., Portland, OR) was used to validate MS/MS based peptide and protein identifications. Peptide identifications were accepted if they could be established at greater than 95.0% probability by the Scaffold Local FDR algorithm. Protein identifications were accepted if they could be established at greater than 99.0% probability to achieve an FDR less than 5.0% and contained at least 3 identified peptides. Protein probabilities were assigned by the Protein Prophet algorithm⁶⁴. Proteins that contained similar peptides and could not be differentiated based on MS/MS analysis alone were grouped to satisfy the principles of parsimony. To estimate OSM induced changes in protein abundance, the Exponentially Modified Protein Abundance Index (emPAI) values of OSM and vehicle treated samples were compared⁶⁵. emPAI provides an

approximate and relative quantitation of the proteins in a mixture based on protein coverage by the peptide matches in a database search result. This method takes into account the fact that more observed peptides will be generated for larger proteins, and for proteins that have many peptides in the preferred mass range for mass spectrometry⁶⁵. Whilst emPAI and other similar spectral counting methods provide only semi-quantitative information, they are highly correlative to protein abundance⁶⁵. EmPAI values were calculated in Scaffold version 4.7.2, in addition to all comparative analysis of OSM and vehicle treated samples and associated statistics.

Deglycosylation of lysosomal proteins

1 μ l 10x Glycoprotein Denaturing Buffer (New England Biolabs) was added to 9 μ l of lysosomal membrane proteins. The glycoproteins were denatured by heating to 95°C for 10 min. Subsequently, 2 μ l 10x G7 Reaction Buffer (New England Biolabs), 2 μ l 10% NP 40 (New England Biolabs) and 1 μ l Peptide -N-Glycosidase F (PNGaseF, New England Biolabs) were added and the reaction volume made up to 20 μ l with H₂O. The reaction mix was incubated at 37°C for 30 min. The deglycosylated protein samples were used for MS or made up in 4x sample buffer and analysed by western blot.

Acknowledgements

All mass-spectrometry and TEM experiments were undertaken at the Cambridge Centre for Proteomics and Cambridge Advanced Imaging Centre (University of Cambridge), respectively. This work was supported by the Medical Research Council [MR/J001023/1 to C.J.W., B.L-L., M.E.D. and T.J.S.].

Conflict of interest

The authors declare that they have no conflicts of interest with the contents of this article.

Author contributions

B.L-L., C.C.K., T.J.S., M.E.D., M.D, J.H., C.J.W. and RF performed all experiments. B.L-L., T.J.S, K.S.L and C.J.W. conceived and designed the experiments. B.L-L. and C.J.W. wrote the manuscript. All authors read and commented on the manuscript. The authors declare that all data supporting the findings of this study are available in the manuscript and its Supplementary Information files, and are

Stat3 alters proteins in the lysosomal membrane

available from the corresponding author upon request.

Bibliography

1. de Duve, C., Pressman, B. C., Gianetto, R., Wattiaux, R. & Appelmans, F. Tissue fractionation studies. 6. Intracellular distribution patterns of enzymes in rat-liver tissue. *Biochem. J.* **60**, 604–617 (1955).
2. Luzio, J. P., Pryor, P. R. & Bright, N. A. Lysosomes: fusion and function. *Nat Rev Mol Cell Biol* **8**, 622–632 (2007).
3. Reddy, A., Caler, E. V & Andrews, N. W. Plasma Membrane Repair Is Mediated by Ca²⁺-Regulated Exocytosis of Lysosomes. *Cell* **106**, 157–169
4. Cox, T. M. & Cachón-González, M. B. The cellular pathology of lysosomal diseases. *J. Pathol.* **226**, 241–254 (2012).
5. Lubke, T., Lobel, P. & Sleat, D. Proteomics of the Lysosome. *Biochim. Biophys. Acta* **1793**, 625–635 (2009).
6. Turk, V. *et al.* Cysteine cathepsins: From structure, function and regulation to new frontiers. *Biochim. Biophys. Acta - Proteins Proteomics* **1824**, 68–88 (2012).
7. Jaquinod, S. K., Chapel, A., Garin, J. & Journet, A. Affinity Purification of Soluble Lysosomal Proteins for Mass Spectrometric Identification. in *Organelle Proteomics* (eds. Pflieger, D. & Rossier, J.) 243–258 (Humana Press, 2008). doi:10.1007/978-1-59745-028-7_17
8. Schröder, B. A., Wrocklage, C., Hasilik, A. & Saftig, P. The proteome of lysosomes. *Proteomics* **10**, 4053–4076 (2010).
9. Sleat, D. E., Valle, M. C. Della, Zheng, H., Moore, D. F. & Lobel, P. The mannose 6-phosphate glycoprotein proteome. *J. Proteome Res.* **7**, 3010–3021 (2008).
10. Sleat, D. E. *et al.* Extending the Mannose 6-Phosphate Glycoproteome by High Resolution/Accuracy Mass Spectrometry Analysis of Control and Acid Phosphatase 5-Deficient Mice. *Mol. Cell. Proteomics* **12**, 1806–1817 (2013).
11. Kollmann, K. *et al.* Identification of novel lysosomal matrix proteins by proteome analysis. *Proteomics* **5**, 3966–3978 (2005).
12. Schwake, M., Schröder, B. & Saftig, P. Lysosomal Membrane Proteins and Their Central Role in Physiology. *Traffic* **14**, 739–748 (2013).
13. Walker, M. W. & Lloyd-Evans, E. Chapter 2 - A rapid method for the preparation of ultrapure, functional lysosomes using functionalized superparamagnetic iron oxide nanoparticles. in *Methods in Cell Biology* (eds. Frances, P. & Nick, P.) **Volume 126**, 21–43 (Academic Press, 2015).
14. Chapel, A. *et al.* An Extended Proteome Map of the Lysosomal Membrane Reveals Novel Potential Transporters. *Mol. Cell. Proteomics* **12**, 1572–1588 (2013).
15. Tulp, A., Verwoerd, D. & Pieters, J. Application of an improved density gradient electrophoresis apparatus to the separation of proteins, cells and subcellular organelles. *Electrophoresis* **14**, 1295–1301 (1993).
16. Christoforou, A. *et al.* A draft map of the mouse pluripotent stem cell spatial proteome. (2016). doi:10.1038/ncomms9992
17. Thul, P. J. *et al.* A subcellular map of the human proteome. *Science* (80-.). (2017).
18. Dietrich, O., Mills, K., Johnson, A. W., Hasilik, A. & Winchester, B. G. Application of magnetic chromatography to the isolation of lysosomes from fibroblasts of patients with lysosomal storage disorders. *FEBS Lett.* **441**, 369–372 (1998).
19. Hildreth, J., Sacks, L. & Hancock, L. W. N-Acetylneuraminic acid accumulation in a buoyant lysosomal fraction of cultured fibroblasts from patients with infantile generalized N-acetylneuraminic acid storage disease. *Biochem. Biophys. Res. Commun.* **139**, 838–844 (1986).
20. Sargeant, T. J. *et al.* Stat3 controls cell death during mammary gland involution by regulating uptake of milk fat globules and lysosomal membrane permeabilization. *Nat. Cell Biol.* **16**, 1057–68 (2014).
21. Becken, U., Jeschke, A., Veltman, K. & Haas, A. Cell-free fusion of bacteria-containing phagosomes with endocytic compartments. *Proc. Natl. Acad. Sci.* **107**, 20726–20731 (2010).
22. Hofmann, D. *et al.* Mass Spectrometry and Imaging Analysis of Nanoparticle-Containing Vesicles Provide a Mechanistic Insight into Cellular Trafficking. *ACS Nano* **8**, 10077–10088 (2014).
23. Tharkeshwar, A. K. *et al.* A novel approach to analyze lysosomal dysfunctions through

Stat3 alters proteins in the lysosomal membrane

- subcellular proteomics and lipidomics: the case of NPC1 deficiency. *Sci. Rep.* **7**, 41408 (2017).
24. Saftig, P., Schröder, B. & Blanz, J. Lysosomal membrane proteins: life between acid and neutral conditions. *Biochem. Soc. Trans.* **38**, 1420 (2010).
 25. Kundra, R. & Kornfeld, S. Asparagine-linked Oligosaccharides Protect Lamp-1 and Lamp-2 from Intracellular Proteolysis. *J. Biol. Chem.* **274**, 31039–31046 (1999).
 26. Appelqvist, H., Waster, P., Kagedal, K. & Ollinger, K. The lysosome: from waste bag to potential therapeutic target. *J. Mol. Cell Biol.* **5**, 214–226 (2013).
 27. Broker, L. E. *et al.* Cathepsin B Mediates Caspase-Independent Cell Death Induced by Microtubule Stabilizing Agents in Non-Small Cell Lung Cancer Cells. *Cancer Res.* **64**, 27 (2004).
 28. Kreuzaler, P. & Watson, C. J. Killing a cancer: what are the alternatives? *Nat Rev Cancer* **12**, 411–424 (2012).
 29. Luke, C. J. *et al.* An Intracellular Serpin Regulates Necrosis by Inhibiting the Induction and Sequelae of Lysosomal Injury. *Cell* **130**, 1108–1119 (2007).
 30. Kreuzaler, P. A. *et al.* Stat3 controls lysosomal-mediated cell death in vivo. *Nat. Cell Biol.* **13**, 303–9 (2011).
 31. Resemann, H. K., Watson, C. J. & Lloyd-Lewis, B. The stat3 paradox: A killer and an oncogene. *Mol. Cell. Endocrinol.* **382**, 603–611 (2014).
 32. Winterbourn, C. C. Toxicity of iron and hydrogen peroxide: the Fenton reaction. *Toxicol. Lett.* **82**, 969–974 (1995).
 33. Imai, K. Characterization of beta-Glucosidase as a Peripheral Enzyme of Lysosomal Membranes from Mouse Liver and Purification. *J. Biochem.* **98**, 1405–1416 (1985).
 34. Schröder, B. *et al.* Integral and Associated Lysosomal Membrane Proteins. *Traffic* **8**, 1676–1686 (2007).
 35. Mellacheruvu, D. *et al.* The CRAPome: a Contaminant Repository for Affinity Purification Mass Spectrometry Data. *Nat. Methods* **10**, 730–736 (2013).
 36. Chen, E. Y. *et al.* Enrichr: interactive and collaborative HTML5 gene list enrichment analysis tool. *BMC Bioinformatics* **14**, 128 (2013).
 37. Kuleshov, M. V *et al.* Enrichr: a comprehensive gene set enrichment analysis web server 2016 update. *Nucleic Acids Res.* **44**, W90–W97 (2016).
 38. Pensa, S. *et al.* Signal transducer and activator of transcription 3 and the phosphatidylinositol 3-kinase regulatory subunits p55?? and p50?? regulate autophagy in vivo. *FEBS J.* **281**, 4557–4567 (2014).
 39. Elbaz-Alon, Y. *et al.* A Dynamic Interface between Vacuoles and Mitochondria in Yeast. *Dev. Cell* **30**, 95–102 (2014).
 40. Hönscher, C. *et al.* Cellular Metabolism Regulates Contact Sites between Vacuoles and Mitochondria. *Dev. Cell* **30**, 86–94 (2014).
 41. Abell, K. *et al.* Stat3-induced apoptosis requires a molecular switch in PI(3)K subunit composition. *Nat. Cell Biol.* **7**, 392–398 (2005).
 42. Otto, P. Grant and Nicholas, J. B. The Roles of flotillin microdomains - endocytosis and beyond. doi:10.1242/jcs.092015
 43. Meister, M. & Tikkanen, R. Endocytic trafficking of membrane-bound cargo: a flotillin point of view. *Membranes (Basel)*. **4**, 356–71 (2014).
 44. Clarkson, R. W. E., Wayland, M. T., Lee, J., Freeman, T. & Watson, C. J. Gene expression profiling of mammary gland development reveals putative roles for death receptors and immune mediators in post-lactational regression. *Breast Cancer Res.* **6**, R92–R109 (2004).
 45. Maley, F., Trimble, R. B., Tarentino, A. L. & Plummer, T. H. Characterization of glycoproteins and their associated oligosaccharides through the use of endoglycosidases. *Anal. Biochem.* **180**, 195–204 (1989).
 46. Lim, C.-Y. & Zoncu, R. The lysosome as a command-and-control center for cellular metabolism. *J. Cell Biol.* **214**, 653 (2016).
 47. Sickmann, A., Mreyen, M. & Meyer, H. E. Identification of Modified Proteins by Mass Spectrometry. *IUBMB Life* **54**, 51–57 (2002).
 48. Johnson, D. E., Ostrowski, P., Jaumouill, V. & Grinstein, S. The position of lysosomes within the cell determines their luminal pH. *J. Cell Biol.* **212**, 677 (2016).

Stat3 alters proteins in the lysosomal membrane

49. Hulsbusch, N., Solis, G. P., Katanaev, V. L. & Stuermer, C. A. O. Reggie-1/Flotillin-2 regulates integrin trafficking and focal adhesion turnover via Rab11a. *Eur. J. Cell Biol.* **94**, 531–545 (2015).
50. Grewal, T., Wason Sundeep, J., Enrich, C. & Rentero, C. Annexins - insights from knockout mice. *Biological Chemistry* **397**, 1031 (2016).
51. Alvarez-Guaita, A. *et al.* Evidence for annexin A6-dependent plasma membrane remodelling of lipid domains. *Br. J. Pharmacol.* **172**, 1677–90 (2015).
52. Shibata, H. *et al.* A New Role for Annexin A11 in the Early Secretory Pathway via Stabilizing Sec31A Protein at the Endoplasmic Reticulum Exit Sites (ERES). *J. Biol. Chem.* **290**, 4981–4993 (2015).
53. Nakamura, H., Jasper, M. J., Hull, M. L., Aplin, J. D. & Robertson, S. A. Macrophages regulate expression of 1,2-fucosyltransferase genes in human endometrial epithelial cells. *Mol. Hum. Reprod.* **18**, 204–215 (2012).
54. Tan, K.-P. *et al.* Fucosylation of LAMP-1 and LAMP-2 by FUT1 correlates with lysosomal positioning and autophagic flux of breast cancer cells. *Cell Death Dis.* **7**, e2347–e2347 (2016).
55. Hara-Nishimura, I. & Hatsugai, N. The role of vacuole in plant cell death. *Cell Death Differ.* **18**, 1298–1304 (2011).
56. Cornillon, S. *et al.* Programmed cell death in Dictyostelium. *J. Cell Sci.* **107**, 2691 (1994).
57. Maltese, W. A. & Overmeyer, J. H. Methuosis: Nonapoptotic Cell Death Associated with Vacuolization of Macropinosome and Endosome Compartments. *Am. J. Pathol.* **184**, 1630–1642 (2014).
58. Reichmann, E., Ball, R., Groner, B. & Friis, R. R. New mammary epithelial and fibroblastic cell clones in coculture form structures competent to differentiate functionally. *J. Cell Biol.* **108**, 1127 (1989).
59. Doench, J. G. *et al.* Optimized sgRNA design to maximize activity and minimize off-target effects of CRISPR-Cas9. *Nat. Biotechnol.* **34**, 184–191 (2016).
60. Sanjana, N. E., Shalem, O. & Zhang, F. Improved vectors and genome-wide libraries for CRISPR screening. *Nat. Methods* **11**, 783–784 (2014).
61. Ran, F. A. *et al.* Genome engineering using the CRISPR-Cas9 system. *Nat. Protoc.* **8**, 2281–2308 (2013).
62. Brinkman, E. K., Chen, T., Amendola, M. & van Steensel, B. Easy quantitative assessment of genome editing by sequence trace decomposition. *Nucleic Acids Res.* **42**, e168 (2014).
63. Schindelin, J. *et al.* Fiji: an open source platform for biological image analysis. *Nat. Methods* **9**, 676–682 (2012).
64. Nesvizhskii, A. I., Keller, A., Kolker, E. & Aebersold, R. A Statistical Model for Identifying Proteins by Tandem Mass Spectrometry. *Anal. Chem.* **75**, 4646–4658 (2003).
65. Ishihama, Y. *et al.* Exponentially Modified Protein Abundance Index (emPAI) for Estimation of Absolute Protein Amount in Proteomics by the Number of Sequenced Peptides per Protein. *Mol. Cell. Proteomics* **4**, 1265–1272 (2005).
66. Reczek, D. *et al.* LIMP-2 Is a Receptor for Lysosomal Mannose-6-Phosphate-Independent Targeting of β -Glucocerebrosidase. *Cell* **131**, 770–783 (2007).
67. Miyaji, T., Omote, H. & Moriyama, Y. Functional characterization of vesicular excitatory amino acid transport by human sialin. *J. Neurochem.* **119**, 1–5 (2011).
68. Lange, P. F., Wartosch, L., Jentsch, T. J. & Fuhrmann, J. C. ClC-7 requires Ostml as a β -subunit to support bone resorption and lysosomal function. *Nature* **440**, 220–223 (2006).
69. Schmidt, K., Wolfe, D. M., Stiller, B. & Pearce, D. A. Cd²⁺, Mn²⁺, Ni²⁺ and Se²⁺ toxicity to *Saccharomyces cerevisiae* lacking YPK9p the orthologue of human ATP13A2. *Biochem. Biophys. Res. Commun.* **383**, 198–202 (2009).
70. Zeevi, D. A., Frumkin, A. & Bach, G. TRPML and lysosomal function. *Biochim. Biophys. Acta - Mol. Basis Dis.* **1772**, 851–858 (2007).
71. Sakata, K. *et al.* Cloning of a lymphatic peptide/histidine transporter. *Biochem. J.* **356**, 53–60 (2001).
72. Schmidt, S., Joost, H.-G. & Schürmann, A. GLUT8, the enigmatic intracellular hexose transporter. *Am. J. Physiol. - Endocrinol. Metab.* **296**, (2009).
73. Baldwin, S. A. *et al.* Functional characterization of novel human and mouse equilibrative

Stat3 alters proteins in the lysosomal membrane

- nucleoside transporters (hENT3 and mENT3) located in intracellular membranes. *J. Biol. Chem.* **280**, 15880–7 (2005).
74. Tabuchi, M., Yoshimori, T., Yamaguchi, K., Yoshida, T. & Kishi, F. Human NRAMP2/DMT1, which mediates iron transport across endosomal membranes, is localized to late endosomes and lysosomes in HEp-2 cells. *J. Biol. Chem.* **275**, 22220–8 (2000).
 75. Falcón-Pérez, J. M. & Dell’Angelica, E. C. Zinc transporter 2 (SLC30A2) can suppress the vesicular zinc defect of adaptor protein 3-depleted fibroblasts by promoting zinc accumulation in lysosomes. *Exp. Cell Res.* **313**, 1473–83 (2007).
 76. Chapuy, B. *et al.* ABC transporter A3 facilitates lysosomal sequestration of imatinib and modulates susceptibility of chronic myeloid leukemia cell lines to this drug. *Haematologica* **94**, 1528–36 (2009).
 77. Demirel, O. *et al.* Identification of a lysosomal peptide transport system induced during dendritic cell development. *J. Biol. Chem.* **282**, 37836–43 (2007).
 78. Rutsch, F. *et al.* Identification of a putative lysosomal cobalamin exporter altered in the cblF defect of vitamin B12 metabolism. *Nat. Genet.* **41**, 234–239 (2009).
 79. Siintola, E. *et al.* The novel neuronal ceroid lipofuscinosis gene MFSD8 encodes a putative lysosomal transporter. *Am. J. Hum. Genet.* **81**, 136–46 (2007).
 80. Fan, X. *et al.* Identification of the gene encoding the enzyme deficient in mucopolysaccharidosis IIIC (Sanfilippo disease type C). *Am. J. Hum. Genet.* **79**, 738–44 (2006).
 81. Friedmann, E. *et al.* SPPL2a and SPPL2b promote intramembrane proteolysis of TNF α in activated dendritic cells to trigger IL-12 production. *Nat. Cell Biol.* **8**, 843–848 (2006).
 82. Pasternak, S. H. *et al.* Presenilin-1, nicastrin, amyloid precursor protein, and gamma-secretase activity are co-localized in the lysosomal membrane. *J. Biol. Chem.* **278**, 26687–94 (2003).
 83. Ungewickell, A. *et al.* The identification and characterization of two phosphatidylinositol-4,5-bisphosphate 4-phosphatases. *Proc. Natl. Acad. Sci. U. S. A.* **102**, 18854–9 (2005).
 84. Pryor, P. R. *et al.* Combinatorial SNARE complexes with VAMP7 or VAMP8 define different late endocytic fusion events. *EMBO Rep.* **5**, 590–5 (2004).
 85. Schieweck, O. *et al.* NCU-G1 is a highly glycosylated integral membrane protein of the lysosome. *Biochem. J.* **422**, (2009).
 86. Chen, F. W., Gordon, R. E. & Ioannou, Y. A. NPC1 late endosomes contain elevated levels of non-esterified (‘free’) fatty acids and an abnormally glycosylated form of the NPC2 protein. *Biochem. J.* **390**, 549–61 (2005).
 87. Chikh, K., Vey, S., Simonot, C., Vanier, M. T. & Millat, G. Niemann–Pick type C disease: importance of N-glycosylation sites for function and cellular location of the NPC2 protein. *Mol. Genet. Metab.* **83**, 220–230 (2004).
 88. Eskelinen, E.-L., Tanaka, Y. & Saftig, P. At the acidic edge: emerging functions for lysosomal membrane proteins. *Trends Cell Biol.* **13**, 137–145 (2003).
 89. Schröder, J. *et al.* Deficiency of the tetraspanin CD63 associated with kidney pathology but normal lysosomal function. *Mol. Cell. Biol.* **29**, 1083–94 (2009).

Stat3 alters proteins in the lysosomal membrane

Table 1: Known lysosomal membrane proteins identified in lysosomal preparations isolated using iron nanoparticles

Published lysosomal membrane proteins identified by mass spectrometry in a preliminary experiment to validate the iron nanoparticle-mediated lysosomal isolation protocol. Associated with Supplementary Table S1.

Protein	Reference	Protein	Reference
H ⁺ -ATPase V1 subunit A	Schröder, B <i>et al</i> ³⁴	LIMP2	Reczek, D. <i>et al</i> ⁶⁶
H ⁺ -ATPase V1 subunit B2	Schröder, B. <i>et al</i> ³⁴	Sialin	Miyaji, T. <i>et al</i> ⁶⁷
H ⁺ -ATPase Vo 116kDa subunit a isoform 1	Schröder, B. <i>et al</i> ³⁴	CLC-7	Lange, P. F. <i>et al</i> ⁶⁸
H ⁺ -ATPase Vo subunit d	Schröder, B. <i>et al</i> ³⁴	ATPase 13A2	Schmidt, K. <i>et al</i> ⁶⁹
H ⁺ -ATPase V1 56/58-kDa subunit B1	Schröder, B. <i>et al</i> ³⁴	Mucolipin-1	Zeevi, D. A. <i>et al</i> ⁷⁰
H ⁺ -ATPase V1 subunit H splice isoform 1	Schröder, B. <i>et al</i> ³⁴	rPHT2	Sakata, K. <i>et al</i> ⁷¹
H ⁺ -ATPase V1 subunit C	Schröder, B. <i>et al</i> ³⁴	GLUT-8	Schmidt, S. <i>et al</i> ⁷²
H ⁺ -ATPase V1 subunit E	Schröder, B. <i>et al</i> ³⁴	Equilibrative nucleoside transporter 3	Baldwin, S. A. <i>et al</i> ⁷³
H ⁺ -ATPase Vo 116kDa subunit a isoform 2	Schröder, B. <i>et al</i> ³⁴	Natural resistance-associated macrophage protein 2	Tabuchi, M. <i>et al</i> ⁷⁴
H ⁺ -ATPase V1 subunit D ^a	Schröder, B. <i>et al</i> ³⁴	Zinc transporter 2	Falcón-Pérez, J.M. <i>et al</i> ⁷⁵
H ⁺ -ATPase V1 subunit G1	Schröder, B. <i>et al</i> ³⁴	ATP-binding cassette subfamily A member 3	Chapuy, B. <i>et al</i> ⁷⁶
S1 accessory proteins (Ac45)	Schröder, B. <i>et al</i> ³⁴	ATP-binding cassette subfamily B member 9	Demirel, O. <i>et al</i> ⁷⁷
H ⁺ -ATPase Vo 16-kDa proteolipid subunit c	Schröder, B. <i>et al</i> ³⁴	Probable lysosomal cobalamin transport	Rutsch, F. <i>et al</i> ⁷⁸
Glucosylceramidase	Schröder, B. <i>et al</i> ³⁴	Major facilitator superfamily domain-containing protein 8	Siintola, E. <i>et al</i> ⁷⁹
Arf-like 10C (Arl8B)	Schröder, B. <i>et al</i> ³⁴	Heparan- α -glucosaminide N-acetyltransferase	Fan, X. <i>et al</i> ⁸⁰
Flotillin 1	Schröder, B. <i>et al</i> ³⁴	Signal peptide peptidase-like 2A	Friedmann, E. <i>et al</i> ⁸¹
Arf-like 10B (Arl8A)	Schröder, B. <i>et al</i> ³⁴	Nicastrin	Pasternak, S. H. <i>et al</i> ⁸²
Lysosomal α -glucosidase	Schröder, B. <i>et al</i> ³⁴	Presenilin1	Pasternak, S. H. <i>et al</i> ⁸²
SLC29A3 nucleoside transporter	Schröder, B. <i>et al</i> ³⁴	Transmembrane protein 55A	Ungewickell, A. <i>et al</i> ⁸³
Chloride Channel 5, CLC5	Schröder, B. <i>et al</i> ³⁴	Transmembrane protein 55B	Ungewickell, A. <i>et al</i> ⁸³
MLN64 N-terminal domain homolog	Schröder, B. <i>et al</i> ³⁴	Vesicle-associated membrane protein 7	Pryor, P. R. <i>et al</i> ⁸⁴
Phospholipase D1 isoform, PLD1A	Schröder, B. <i>et al</i> ³⁴	Transmembrane protein 192	Schröder, B. <i>et al</i> ³⁴
Endothelin-converting enzyme 1 isoform B	Schröder, B. <i>et al</i> ³⁴	Lysosomal protein NCU-G1	Schieweck, O. <i>et al</i> ⁸⁵

Stat3 alters proteins in the lysosomal membrane

C18orf8 protein, Mic1	Schröder, B. <i>et al</i> ³⁴	Transmembrane protein 63A	Schröder, B. A. <i>et al</i> ⁸
SID1 transmembrane protein, SIDT2	Schröder, B. <i>et al</i> ³⁴	Niemann-Pick C1 protein	Chen, F.W. <i>et al</i> ⁸⁶
GPR137 protein	Schröder, B. <i>et al</i> ³⁴	Niemann-Pick C2 protein	Chikh, K. <i>et al</i> ⁸⁷
LAMP1	Eskelinen, E-L. <i>et al</i> ⁸⁸	Osteopetrosis-associated transmembrane protein 1	Lange, P. F. <i>et al</i> ⁶⁸
LAMP2	Eskelinen, E-L. <i>et al</i> ⁸⁸		
CD63/LIMP1	Schröder, J. <i>et al</i> ⁸⁹		

Stat3 alters proteins in the lysosomal membrane

Table 2. Proteins identified by MS in control (vehicle) or OSM treated lysosomal preparations only

Associated with Figure 4 and Supplementary tables S4, S6 and S7.

	Accession	Gene symbol	Protein Name
Vehicle only	Q8VDV8	Mitd1	MIT domain-containing protein 1
	Q9WVE8	Pacsin2	Protein kinase C and casein kinase substrate in neurons protein 2
	Q8BHL4	Gprc5a	Retinoic acid-induced protein 3
OSM only	Q80X90	Flnb	Filamin-B
	Q9EPR5	Sorcs2	VPS10 domain-containing receptor SorCS2
	Q8BKG3	Ptk7	Inactive tyrosine-protein kinase 7
	P40124	Cap1	Adenylyl cyclase-associated protein 1
	Q91V01	Lpcat3	Lysophospholipid acyltransferase 5
	P48678	Lmna	Prelamin-A/C
	Q61738	Itga7	Integrin alpha-7
	Q91V92	Acly	ATP-citrate synthase
	Q91VS7	Mgst1	Microsomal glutathione S-transferase 1
	Q8BU30	Iars	Isoleucine--tRNA ligase, cytoplasmic
	O70309	Itgb5	Integrin beta-5
	Q80VQ0	Aldh3b1	Aldehyde dehydrogenase family 3 member B1
	P35821	Ptpn1	Tyrosine-protein phosphatase non-receptor type 1
	O70133	Dhx9	ATP-dependent RNA helicase A
	Q9DBG3	Ap2b1	AP-2 complex subunit beta
	P14901	Hmox1	Heme oxygenase 1
	Q6P9J9	Ano6	Anoctamin-6
	Q8BTM8	Flna	Filamin-A
	Q61739	Itga6	Integrin alpha-6
	P97384	Anxa11	Annexin A11
Q62261	Sptbn1	Spectrin beta chain, non-erythrocytic 1	

Stat3 alters proteins in the lysosomal membrane

Table 3. Proteins that were differentially represented in OSM treated lysosomal preparations.

16 (pink) and 23 (blue) proteins were differentially represented in control and OSM treated samples respectively (depicted in Fig. 4C). Many lysosomal enzymes were decreased by OSM, whilst the lysosomal localisation of cell surface and cytoskeletal components were increased. Proteins that were absent/near absent from the comparator sample (INF or 0) are not plotted in Fig. 4F.

Name	Symbol	Accession Number	p-value (T-TEST)	Fold Change: OSM/veh (emPAI)
MIT domain-containing protein 1 OS	Mitd1	Q8VDV8	0.034	0
Epoxide hydrolase 1 OS	Ephx1	Q9D379	0.015	0.06
Galactocerebrosidase OS	Galc	P54818	0.0021	0.09
Palmitoyl-protein thioesterase 1 OS	Ppt1	O88531	0.00089	0.1
Acid ceramidase OS	Asah1	Q9WV54	0.014	0.1
E3 ubiquitin-protein ligase RNF13 OS	Rnf13	O54965	0.043	0.1
CD82 antigen OS	Cd82	P40237	0.0091	0.2
Beta-hexosaminidase subunit beta OS	Hexb	P20060	0.022	0.2
Lysosomal alpha-mannosidase OS	Man2b1	O09159	0.014	0.3
IST1 homolog OS	Ist1	Q9CX00	0.019	0.3
Beta-glucuronidase OS	Gusb	P12265	0.047	0.3
Lactadherin OS	Mfge8	P21956	0.0067	0.4
Ras-related protein Rab-18 OS	Rab18	P35293	0.025	0.4
Claudin-3 OS	Cldn3	Q9Z0G9	0.011	0.5
Retinoid-inducible serine carboxypeptidase OS	Scepe1	Q920A5	0.014	0.5
Sideroflexin-1 OS	Sfxn1	Q99JR1	0.046	0.5
Lysosome-associated membrane glycoprotein 2 OS	Lamp2	P17047	0.003	1.5
Integrin beta-1 OS	Itgb1	P09055	0.017	2.2
Monocarboxylate transporter 1 OS	Slc16a1	P53986	0.022	2.5
Basigin OS	Bsg	P18572	0.0017	3.1
Importin subunit beta-1 OS	Kpnb1	P70168	0.0026	3.5
Annexin A1 OS	Anxa1	P10107	0.0051	4.3
ADP-ribosyl cyclase 2 OS	Bst1	Q64277	0.022	4.5
Catenin delta-1 OS	Ctnnd1	P30999	0.013	4.9
Annexin A6 OS	Anxa6	P14824	0.0025	5.8
Junction plakoglobin OS	Jup	Q02257	0.023	8.1
Talin-1 OS	Tln1	P26039	0.032	8.5
Flotillin-1 OS	Flot1	O08917	0.036	8.7
Keratin, type II cytoskeletal 8 OS	Krt8	P11679	0.0016	9.3
T-complex protein 1 subunit beta OS	Cct2	P80314	0.018	9.6
Vinculin OS	Vcl	Q64727	0.027	12
Protein-glutamine gamma-glutamyltransferase 2 OS	Tgm2	P21981	0.044	14
Microsomal glutathione S-transferase 1 OS	Mgst1	Q91VS7	0.0049	INF
Filamin-A OS	Flna	Q8BTM8	0.0056	INF
Integrin alpha-6 OS	Itga6	Q61739	0.027	INF
Annexin A11 OS	Anxa11	P97384	0.028	INF
Filamin-B OS	Flnb	Q80X90	0.041	INF
Integrin alpha-7 OS	Itga7	Q61738	0.041	INF
Inactive tyrosine-protein kinase 7 OS	Ptk7	Q8BKG3	0.042	INF

Figure legends

Figure 1. Iron nanoparticle mediated isolation of EpH4 cell lysosomes.

A, Transmission electron microscopy (TEM) of EpH4 cells showing iron nanoparticles residing in degradative lysosomal vacuoles (arrow head) or in lysosomal vacuoles devoid of degradative material (arrow). Scale bars: 500 nm. **B**, Brightfield microscopy and quantification of iron nanoparticle-induced cell death of EpH4 cells, observed solely in the presence of hydrogen peroxide (H_2O_2). EpH4 cells were treated with H_2O_2 for 19 h. Scale bars: 25 μ m. **C**, Schematic of the magnetic iron nanoparticle lysosomal purification protocol. Adapted from Sargeant, Lloyd-Lewis *et al*, 2014²⁰. **D**, TEM of lysosomes (top panel) and of negatively stained lysosomes (bottom panel) isolated using the magnetic iron nanoparticle purification protocol. Arrowheads mark areas containing iron nanoparticles. Arrows indicate unidentifiable membranous fragments, which may be endo-lysosomal tubules or remnants from the ER or Golgi apparatus. Scale bars: 500 nm. **E**, Isolated EpH4 lysosomes are predominantly clear of mitochondria. EpH4 cells were labelled with 10 kDa FITC-dextran (2.5 mg/ml, green) with (Mag +) or without (Mag -) iron nanoparticle containing media for 2 h and subsequently stained with MitoTrackerTM (500 nm, red) for 30 min prior to isolation. Representative images of the post nuclear supernatant (PNS), post magnetic supernatant (SN) and of the magnetic lysosomal pellet (LP) of the two conditions are shown. Scale bar: 10 μ m. **F**, Isolated EpH4 lysosomes are highly pure with undetectable contamination from other organelles as observed by immunoblotting. N, nuclear lysate. Organelle marker proteins: LAMP2, lysosomes; ERp57, endoplasmic reticulum; GAPDH, cytoplasm; Rab5, early endosomes; Cox IV, mitochondria; Histone H3, nucleus.

Figure 2. Membrane fractionation of isolated EpH4 lysosomes.

A, Hypotonic lysis of iron nanoparticle isolated lysosomes from EpH4 cells to separate the lysosomal membranes (LM) from the lysosomal content (LC). LAMP2 immunoblotting shows its enrichment in the LM fraction. Ctsl, cathepsin L (single chain: sc; double chain: dc); PNS, post nuclear supernatant; SN, post magnetic supernatant. **B**, Cathepsin activity in EpH4 lysosomes isolated using iron nanoparticles and extracted using TX-100 (total lysosomal content, TX+) or by hypotonic lysis and fractionation (membrane fractions: LM+, matrix: LC+) compared to unlabelled control samples (TX-, LM- and LC-). **C, D**, Freeze thawing of lysosomes improved lysosome membrane separation from the lysosomal matrix. Cathepsin (**C**) and β -glucuronidase activity (**D**) in the LC fraction is shown as a fold of LM.

Figure 3. OSM induces vesicular biogenesis in EpH4 cells.

A, Immunoblot showing OSM induced expression of p55 α /p50 α and cathepsin B (Ctsb; sc, single chain) downstream of activated Stat3 signalling in EpH4 cells. **B**, Brightfield microscopy showing OSM induced vacuolisation in EpH4 cells treated for 72 h. Scale bars: 25 μ m. **C**, TEM images showing an increased number of degradative vesicles after 72 h of OSM stimulation. Scale bars: 500 nm. **D**, Fluorescence microscopy of LysoTracker[®] accumulation in cells treated with OSM for 72 h. Scale bars: 20 μ m. **E**, Western blot analysis of LAMP2 and cathepsin L in fractionated lysosomes isolated from vehicle and OSM stimulated (72 h) cells using iron nanoparticles. Post nuclear supernatant (PNS), lysosomal membrane fraction (LM), single chain cathepsin L (sc Ctsl), heavy chain of the double-chain form of cathepsin L (dc Ctsl). **F**, Graph showing increased cathepsin activity in LC and LM fractions from OSM stimulated cells.

Figure 4. OSM induced changes in the lysosomal proteome of EpH4 cells.

A, Western blot analysis of LAMP2 and cathepsin L in fractionated lysosomes isolated from vehicle and OSM stimulated (72 h) cells and submitted for MS analysis. A representative blot from three independent experiments is presented. Post nuclear supernatant (PNS), lysosomal content fraction (LC), lysosomal membrane fraction (LM), single chain cathepsin L (sc Ctsl), heavy chain of the double-chain form of cathepsin L (hc Ctsl). **B**, Immunoblotting for organelle marker proteins in lysosomal preparations isolated from control and OSM stimulated EpH4 cells. ERp57, endoplasmic reticulum; GAPDH, cytoplasm; Rab5, early endosomes; Cox IV, mitochondria; Histone H3, nucleus. A representative blot from three independent experiments is presented. For Cox IV immunoblotting, blots from two different replicates are shown, revealing slight contamination in one replicate. **C**, Analysis

Stat3 alters proteins in the lysosomal membrane

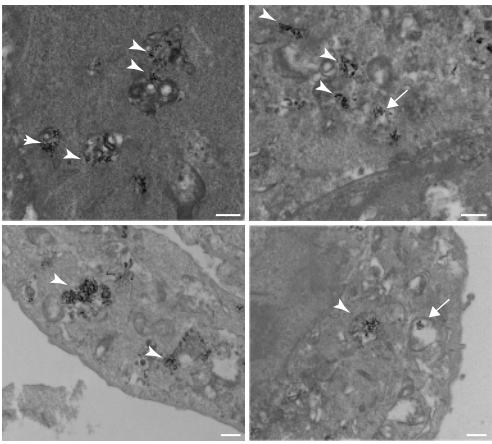
pipeline of mass spectrometry results obtained from lysosomes isolated from vehicle and OSM (72 h) treated EpH4 cells. 3 independent biological repeats were undertaken per condition, and each replicate included an unlabeled control samples (9 preparations in total). **D**, Significantly enriched KEGG (2016) pathways derived from MS analysis of EpH4 lysosomal preparations isolated using iron nanoparticles. **E**, Significant GO annotations of proteins according to cellular component, derived from mass-spectrometry analysis of EpH4 lysosomal preparations isolated using iron nanoparticles. For inclusion in the analysis undertaken in **D** and **E**, proteins were required to be identified in at least 5 out of 6 independent runs (3 veh, 3 OSM). **F**, Volcano plot showing the fold change in emPAI values induced by OSM stimulation. Proteins that were significantly changed by OSM treatment are shown in green (T-Test, $p < 0.05$)

Figure 5. Stat3 mediated regulation of the lysosomal compartment

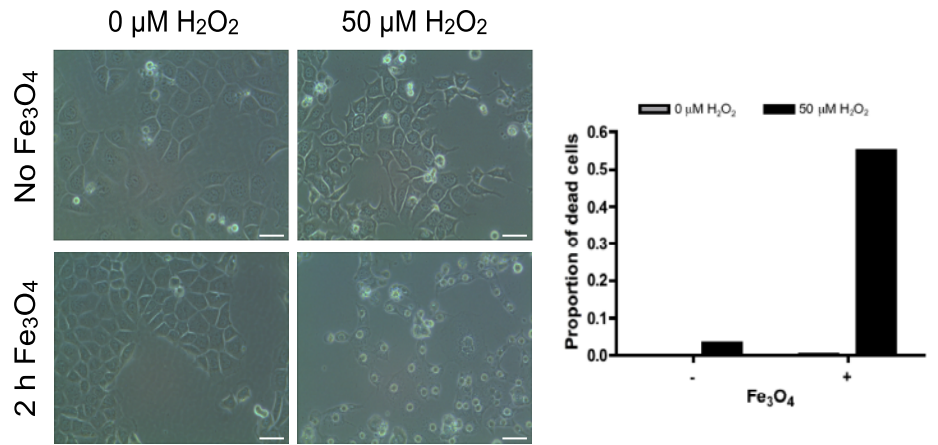
A, Western blot validation of the lysosomal localisation of flotillin 1 and flotillin 2 in iron nanoparticle isolated EpH4 lysosomes (Mag+) after 72 h OSM stimulation. Post nuclear supernatant (PNS). White asterisk indicates the expected molecular weight of flotillin 2. Representative blots of n=3 (flotillin 1) and n=2 (flotillin 2) independent experiments are shown. **B**, Microarray analysis of twelve different timepoints during the mammary gland pregnancy cycle showing the involution related expression profiles of flotillin 1 and flotillin 2. V, virgin; d G, days gestation; d L, days lactation; h I, hours involution. **C**, Fluorescence microscopy of LAMP1 and LAMP2 immunostaining in EpH4 cells treated with OSM for 72 h. Scale bars: 10 μm . **D**, Western blot analysis of OSM induced changes to the lysosomal proteins LAMP1, LAMP2, CD63, and cathepsin B in whole cell lysates from normal (WT) and two independent Stat3 KO EpH4 cell lines after 72 h of stimulation. Proteins were separated by SDS-PAGE under reducing or non-reducing conditions as indicated. Pro form of cathepsin B (pro-Ctsb), single chain cathepsin B (sc Ctsb), scrambled sgRNA control EpH4 cells (Scram). **E**, Microarray analysis of twelve different timepoints during the mammary gland pregnancy cycle showing the involution related expression profiles of CD63 and LAMP2.

Figure 1

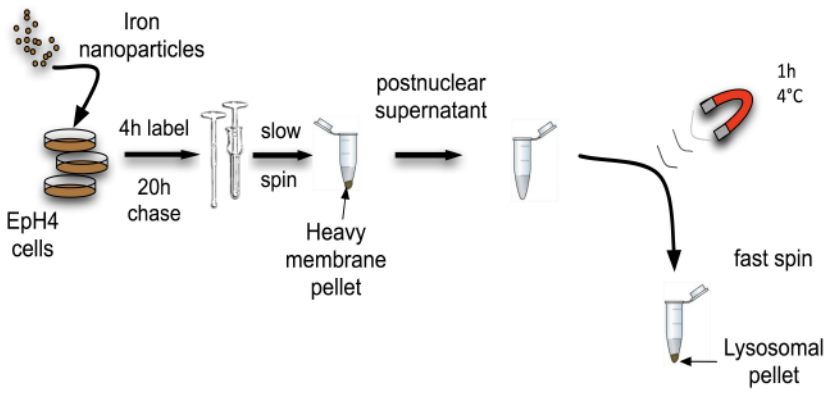
A



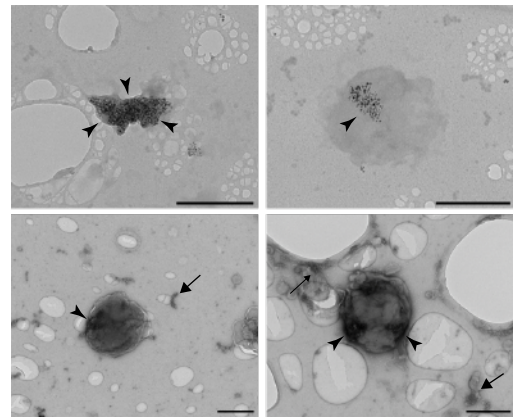
B



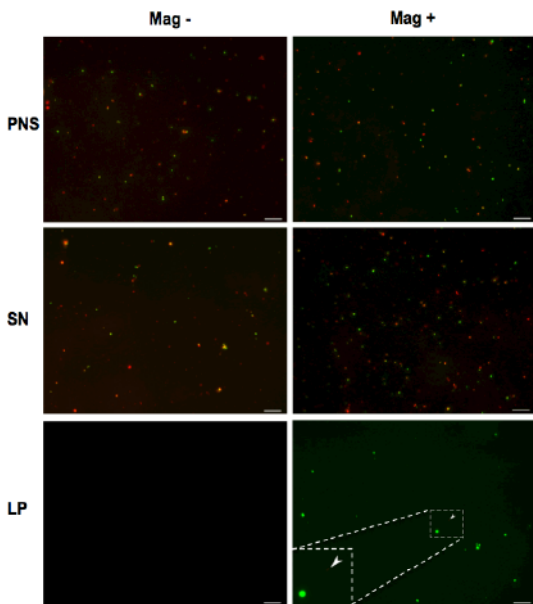
C



D



E



F

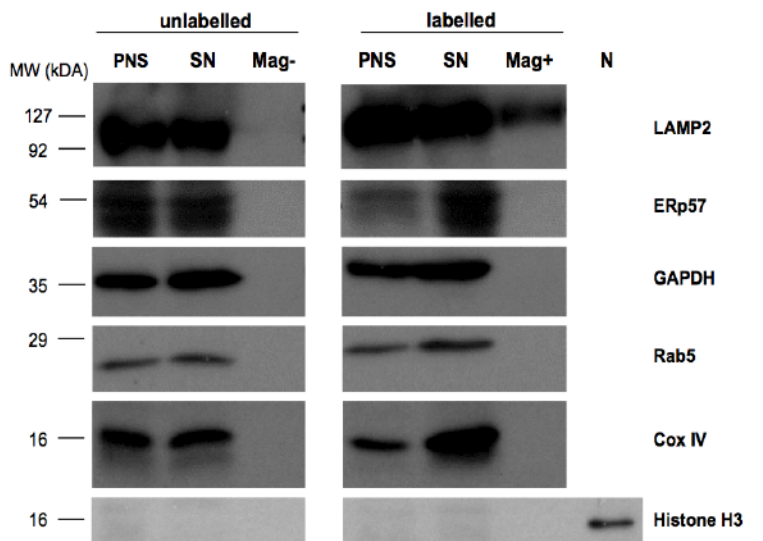


Figure 2

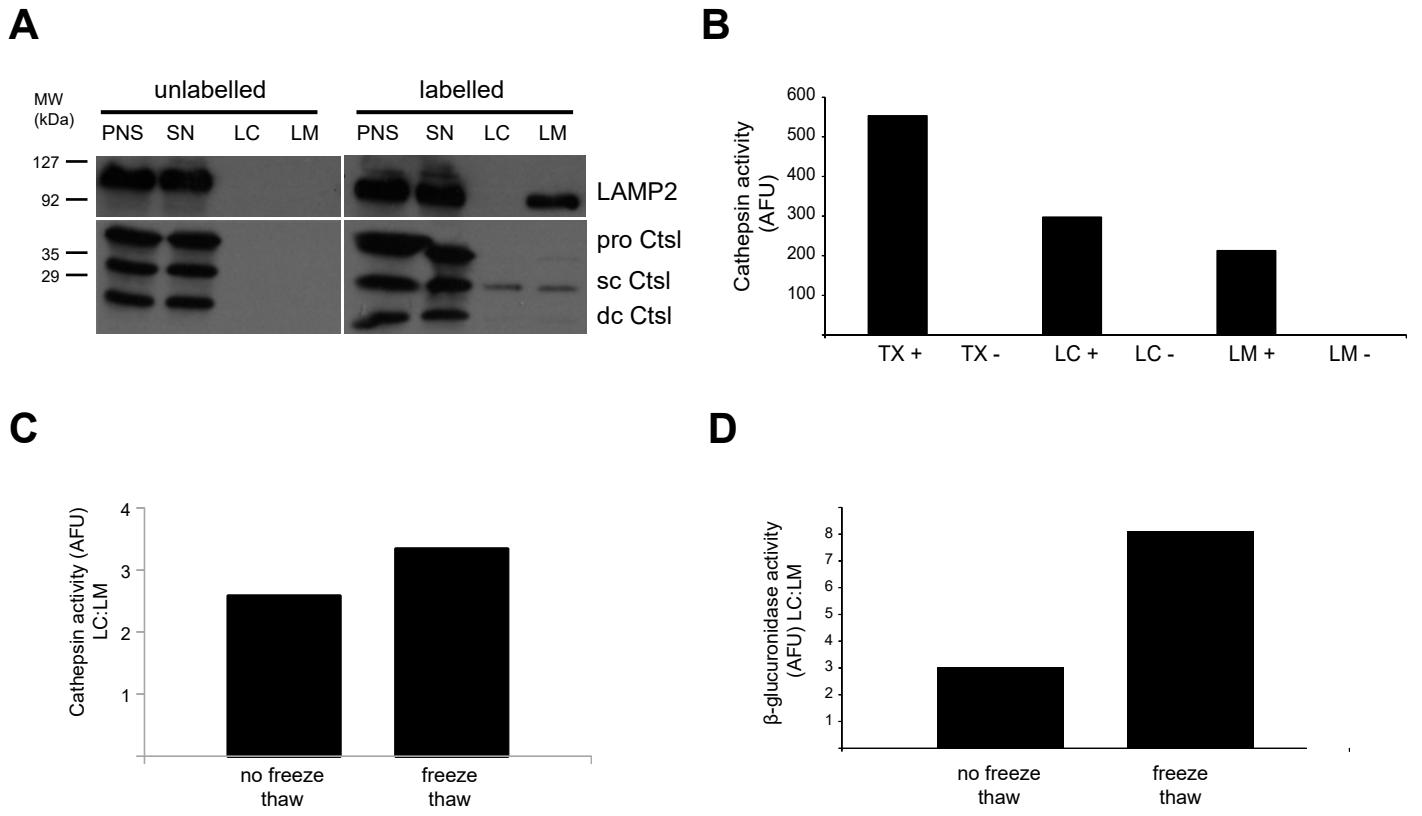
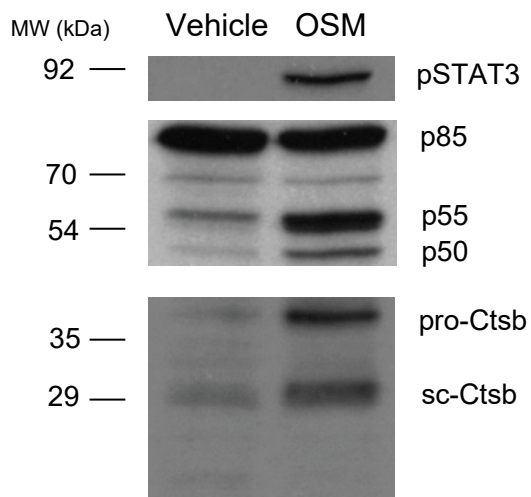
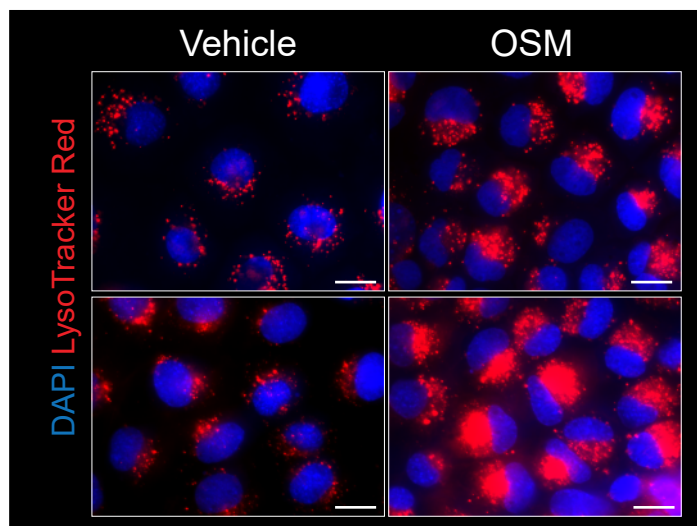


Figure 3

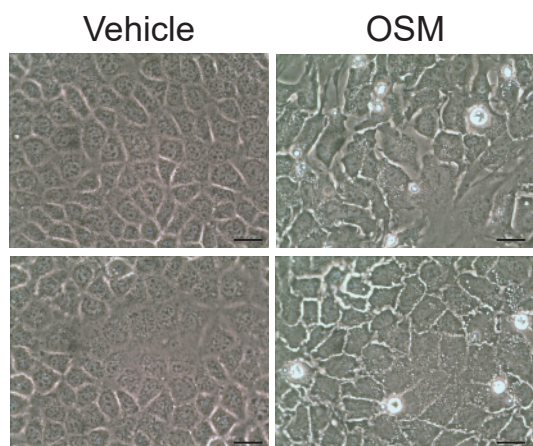
A



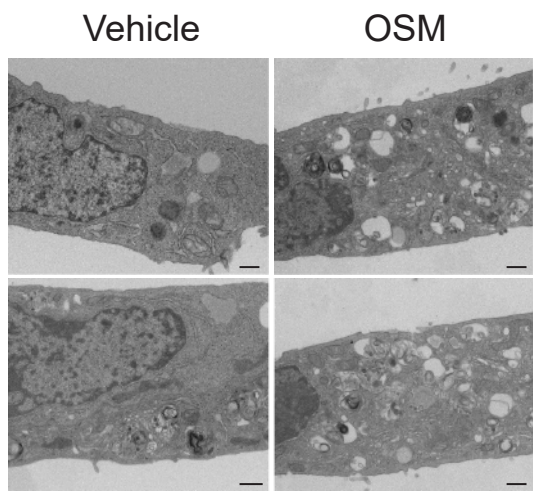
D



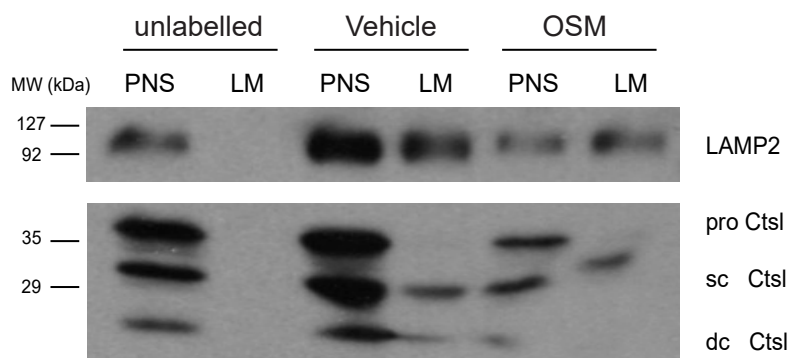
B



C



E



F

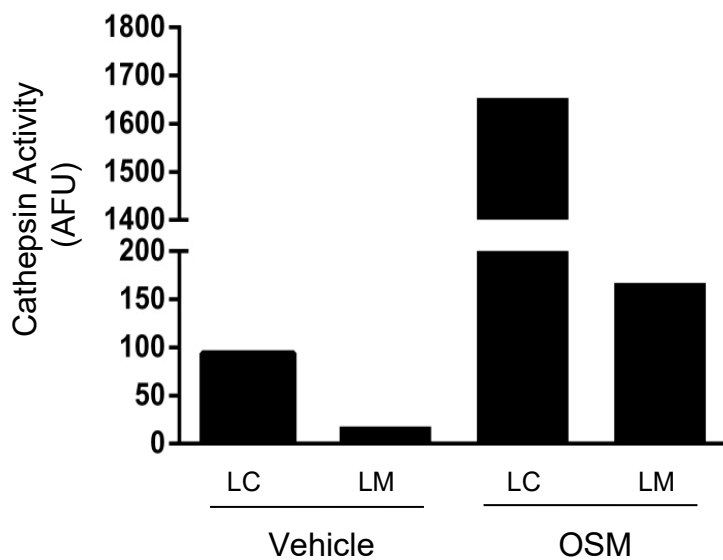


Figure 4

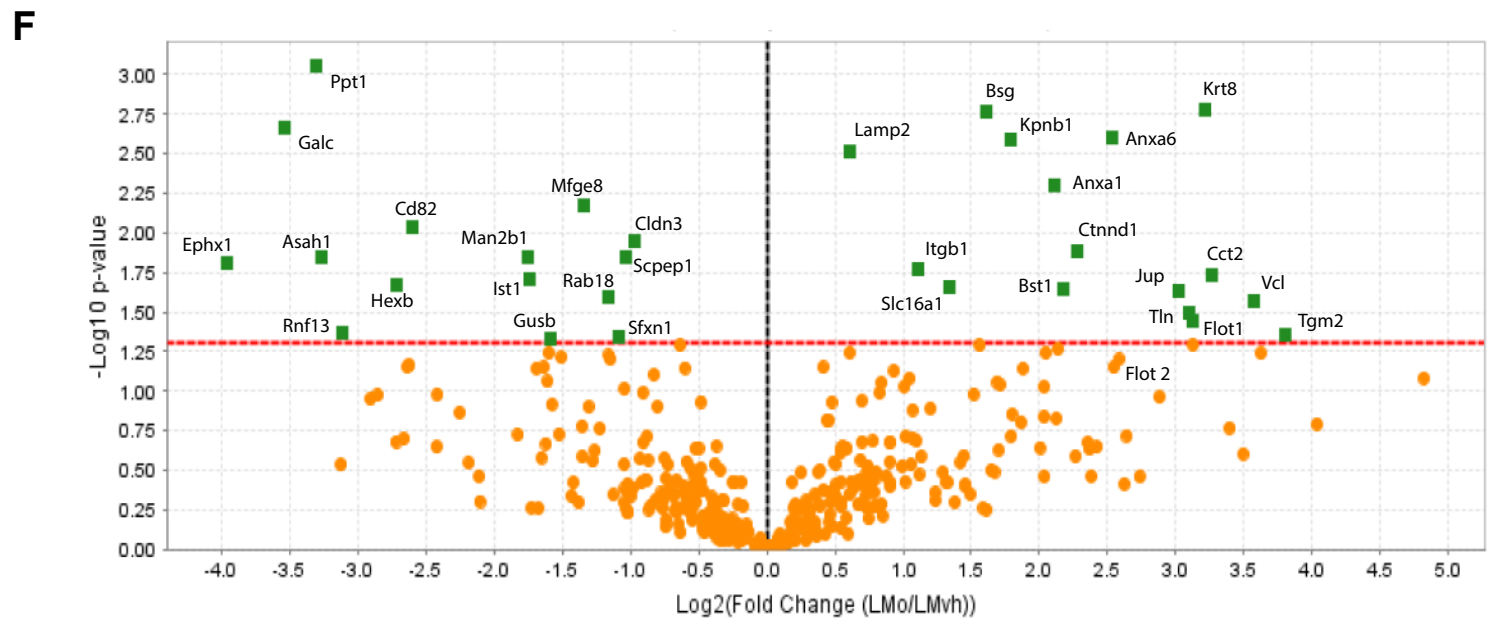
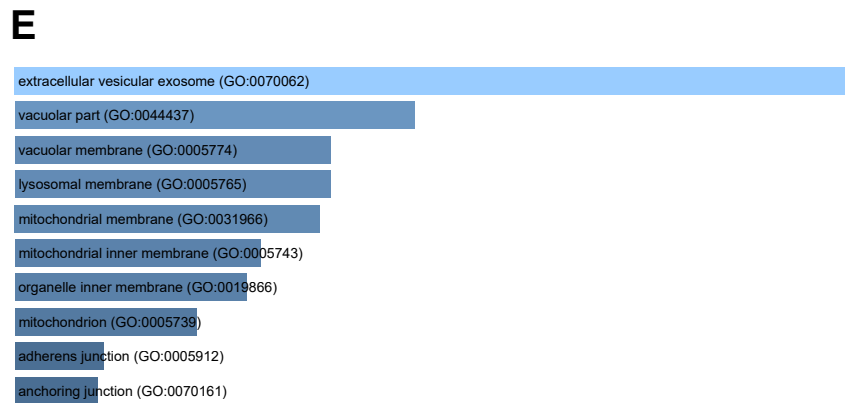
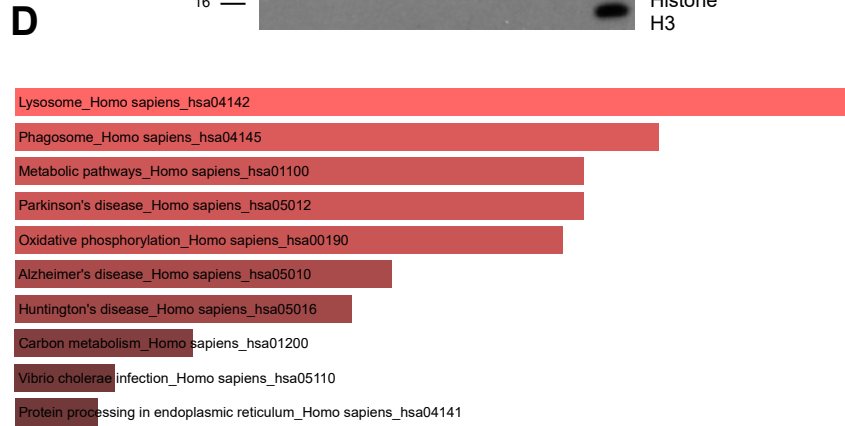
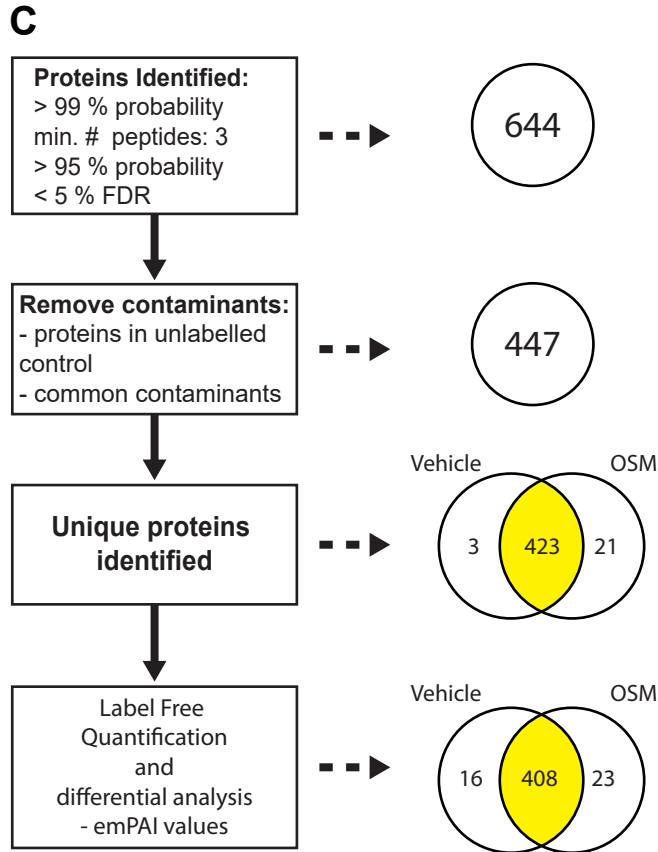
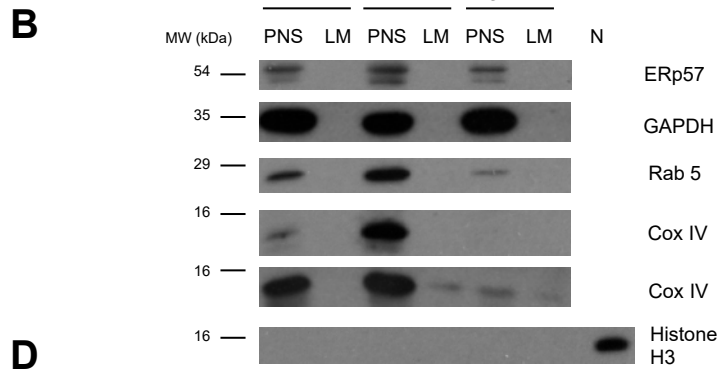
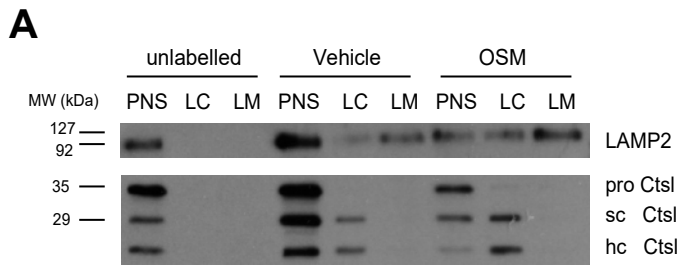


Figure 5

